

5-2-2018

Investigation of Low-Temperature Effects on DNA Photocleavage Using a Novel Thioether Substituted Cyanine Dye

Andrew Clay
aclay7@student.gsu.edu

Follow this and additional works at: https://scholarworks.gsu.edu/chemistry_theses

Recommended Citation

Clay, Andrew, "Investigation of Low-Temperature Effects on DNA Photocleavage Using a Novel Thioether Substituted Cyanine Dye." Thesis, Georgia State University, 2018.
https://scholarworks.gsu.edu/chemistry_theses/113

This Thesis is brought to you for free and open access by the Department of Chemistry at ScholarWorks @ Georgia State University. It has been accepted for inclusion in Chemistry Theses by an authorized administrator of ScholarWorks @ Georgia State University. For more information, please contact scholarworks@gsu.edu.

INVESTIGATION OF LOW-TEMPERATURE EFFECTS ON DNA
PHOTOCLEAVAGE USING A NOVEL THIOETHER SUBSTITUTED CYANINE DYE

by

ANDREW C. CLAY

Under the Direction of Kathryn B. Grant, Ph.D.

ABSTRACT

The implications of temperature effects on photochemical processes when it comes to near-infrared DNA photosensitizing agents are discussed in addition to the unique spectroscopic features of a sulfur meso-substituted heptamethine cyanine dye relative to oxygen and nitrogen analogues. Specifically, reactive oxygen scavenger experiments, preliminary kinetic data, and absorption spectra are considered in this continued investigation. Additionally, binding and stability studies indicate that the general structure of the cyanine dye can be further optimized to potentially improve DNA photocleavage yields at physiological temperatures while employing the exceptional properties of sulfur-incorporated polymethine dyes.

INDEX WORDS: cyanine dye, photocleavage, sulfur, thioether, low-temperature effects, sulfur radicals, photodynamic therapy

INVESTIGATION OF LOW-TEMPERATURE EFFECTS ON DNA
PHOTOCLEAVAGE USING A NOVEL THIOETHER SUBSTITUTED CYANINE DYE

by

ANDREW C. CLAY

A Thesis Submitted in Partial Fulfillment of the Requirements for the Degree of

Master of Science

in the College of Arts and Sciences

Georgia State University

2018

Copyright by
Andrew C. Clay
2018

INVESTIGATION OF LOW-TEMPERATURE EFFECTS ON DNA
PHOTOCLEAVAGE USING A NOVEL THIOETHER SUBSTITUTED CYANINE DYE

by

ANDREW C. CLAY

Committee Chair: Kathryn B. Grant

Committee: Maged Henary

Donald Hamelberg

Electronic Version Approved:

Office of Graduate Studies

College of Arts and Sciences

Georgia State University

December 2017

DEDICATION

I am dedicating this to my entire family but particularly my late aunt Judith Hunter Campbell Sychak. I lost her before I began my first year of college, but she has continued to affect my decision-making in the most positive way even after leaving us. This is for you.

ACKNOWLEDGEMENTS

I want to thank my committee members, Dr. Maged Henary and Dr. Donald Hamelberg, for their assistance and prolonged involvement over the course of my thesis and defense. I would like to acknowledge my research advisor Dr. Kathryn B. Grant for her persistent encouragement and guidance through this process. My continued passion for science was largely instilled by her compassion and unwavering motivation to pursue research and knowledge. Additionally, I would like to acknowledge my fellow lab associates who were always there to help troubleshoot, assist one another, and come together for a nice cup of joe every now and then. I was fortunate enough to be a part of such a cohesive yet diverse group of people.

My parents, Donald and Deborah Clay, and the rest of my family have supported me throughout my entire education without hesitation. They have inspired me more than I can communicate on a page in my thesis. I would especially like to thank my friends for their words of wisdom in troubled times and always being there to help unwind after stressful situations. I would also like to thank my “squeak squad” for a great summer – thanks for all the P&R!

Lastly, I would like to acknowledge all the educators who have impacted my life (Dr. Kathryn B. Grant, Dr. Alfonso Baumstark, Dr. Cara Minardi, Karen Wright, Alan Sears, Beth Villemez, Dr. Larry Lynch, and so many more). Thank you for the unceasing inspiration and imparted wisdom that I have used countless times outside of the classroom.

“The function of education is to teach one to think intensively and to think critically. Intelligence plus character – that is the goal of true education.” – Dr. Martin Luther King, Jr.

TABLE OF CONTENTS

| | |
|---|-----------|
| ACKNOWLEDGEMENTS | V |
| LIST OF TABLES | IX |
| LIST OF FIGURES | X |
| 1 INTRODUCTION..... | 1 |
| 1.1 Cyanine Dyes | 1 |
| <i>1.1.1 General Structure and Modifications.....</i> | <i>1</i> |
| <i>1.1.2 Aggregation</i> | <i>4</i> |
| <i>1.1.3 DNA Binding and Interaction</i> | <i>4</i> |
| 1.2 Photosensitizers | 5 |
| <i>1.2.1 Photodynamic Therapy</i> | <i>7</i> |
| <i>1.2.2 Reactive Oxygen Species.....</i> | <i>8</i> |
| <i>1.2.3 Advantages of Sulfur-substituted Photosensitizers.....</i> | <i>9</i> |
| 1.3 Low-Temperature Effects | 11 |
| <i>1.3.1 Temperature Effects on Nonradiative Processes</i> | <i>12</i> |
| <i>1.3.2 Temperature Effects on Photobleaching</i> | <i>14</i> |
| 1.4 Summary of Research..... | 15 |
| 2 EXPERIMENT | 16 |
| 2.1 Materials and Instrumentation..... | 16 |
| 2.2 Methods..... | 17 |

| | | |
|-------|--|----|
| 2.2.1 | <i>UV-Visible Spectrophotometry</i> | 17 |
| 2.2.2 | <i>Circular Dichroism</i> | 19 |
| 2.2.3 | <i>Fluorescence Spectroscopy</i> | 20 |
| 2.2.4 | <i>Gel Electrophoresis</i> | 20 |
| 3 | RESULTS | 26 |
| 3.1 | UV/Visible Spectrophotometry | 26 |
| 3.1.1 | <i>Absorbance Spectra in DMSO</i> | 27 |
| 3.1.2 | <i>Absorbance Spectra with CT-DNA</i> | 29 |
| 3.1.3 | <i>Temperature Effects on Aggregation and Absorbance</i> | 31 |
| 3.1.4 | <i>Photobleaching at Decreasing Temperature</i> | 32 |
| 3.2 | Fluorescence Spectroscopy | 33 |
| 3.3 | CD Spectroscopy | 35 |
| 3.4 | Photocleavage Experiments | 36 |
| 3.4.1 | <i>Decreasing Temperature Photocleavage Experiment</i> | 36 |
| 3.4.2 | <i>Photocleavage Titration</i> | 38 |
| 3.4.3 | <i>Scavenger Experiments and Argon Purging</i> | 42 |
| 3.4.4 | <i>Binding Mode Investigation via Photocleavage Inhibition</i> | 45 |
| 4 | CONCLUSIONS | 47 |
| | REFERENCES | 50 |
| | APPENDIX | 53 |

LIST OF TABLES

| | |
|---|----|
| Table 2.1: Photocleavage concentration titration was prepared with the below concentrations of Dye 1..... | 21 |
| Table 2.2: The initial kinetics experiment was set up with the following times and controls..... | 22 |
| Table 2.3: The first experiment used to optimize concentration and irradiation times for the preliminary kinetics experiments..... | 22 |
| Table 2.4: The setup for the four trials of the photocleavage with decreasing temperatures experiment using Dye 1 can be seen below..... | 23 |
| Table 2.5: For each scavenger experiment the various controls and samples were prepared as below..... | 24 |
| Table 2.6: The below setup for the argon purging experiment was used to determine the effects oxygen may have in the photocleavage mechanism..... | 25 |
| Table 2.7: The inhibitors consisted of methyl green (M), ethidium bromide (E), and pentamidine (P). Dye 1 (D) was equilibrated in rows 4-6 first and equilibrated in rows 7-9 last..... | 25 |

LIST OF FIGURES

| | |
|--|----|
| Figure 1-1: General structure of symmetrical cyanine dyes. | 2 |
| Figure 1-2: The structures of the cyanine dyes that are compared and investigated in this paper. Dyes 1 and 3 were synthesized by Xiaozhong Ma and Dye 2 was synthesized by Andy Levitz, under the direction of Dr. Maged Henary. | 3 |
| Figure 1-3: This illustrates the Jablonski diagram in relation to generating reactive oxygen species through Type I and Type II energy transfer pathways. Nonradiative pathways (intersystem crossing and internal conversion) are also shown. | 6 |
| Figure 1-4: The structure of profimer sodium (Photofrin®), a current FDA approved photosensitizer that absorbs red light. | 7 |
| Figure 1-5: The box illustrates the absorption region that represents the PDT therapeutic window. This is located between absorption by ubiquitous biomolecules (UV/visible region) and water, which absorbs in the infrared region. ¹⁴ | 8 |
| Figure 1-6: This graph shows the cell-survival curves for both hypoxic and aerobic cells receiving radiosensitizer doses that result in the same fraction of surviving cells. Higher doses are needed for hypoxic cells due to the lack of available oxygen. ²¹ The SI unit Gy (Gray) is equivalent to the absorption of one joule of radiation energy per kg. | 10 |
| Figure 1-7: This form of the Jablonski diagram illustrates the competitive pathway of vibrational relaxation through internal conversion in regards to other photochemical processes. Abbreviations: k_V stands for the vibrational relaxation or internal conversion rate constant, k_{PC} stands for the photochemistry rate constant. ²⁹ | 12 |
| Figure 3-1: This figure shows the changes in aggregation over time in DMSO for 10 μ M of Dyes 1-3 . Absorption spectra recorded in 5 min increments. | 26 |

- Figure 3-2: The absorption spectra of Dyes **1-3** in DMSO at $t = 0$ min (all dye concentrations were $10 \mu\text{M}$). All molar extinction coefficients are rough estimates based on the above trials only. 28
- Figure 3-3: The absorption spectra of Dyes **1** and **2** in methanol at $t = 0$ min (both dye concentrations were $5 \mu\text{M}$). Both molar extinction coefficients are rough estimates based on the above trials only. 28
- Figure 3-4: The absorption spectra of $10 \mu\text{M}$ Dye **1** in the presence and absence of CT-DNA ($150 \mu\text{M}$ bp). There is a slight red-shift and hypochromicity in the Dye-DNA complex spectrum when compared to the dye absorption spectrum in 10 mM phosphate buffer pH 7.0..... 29
- Figure 3-5: The CT-DNA titration with Dye **1** in a 10 mM phosphate buffer pH 7.0 shows a sharp absorption decrease at slightly below $60 \mu\text{M}$ bp CT-DNA. All concentrations of CT-DNA were corrected for sample dilutions..... 30
- Figure 3-6: Temperature effects on absorbance and aggregation were determined to see if any difference could explain possible increases in photocleavage yields at low temperatures. Dye **1** ($5 \mu\text{M}$) in the presence of $60 \mu\text{M}$ bp CT-DNA and 10 mM phosphate buffer pH 7.0 subjected to 2°C and 24°C for 10 min before spectra were immediately obtained. A total of four trials were done at 2°C and three at 24°C with consistent results between each trial. An obvious decrease in the DNA-dye complex absorption spectra is visible at 2°C 31
- Figure 3-7: The absorption spectra before and after irradiation (780 nm with 83 mW for 3 min) at room temperature and dry ice conditions which show the degree of photobleaching under the different temperatures. All samples contained $60 \mu\text{M}$ bp CT-DNA, 10 mM phosphate

- buffer pH 7.0, and 5 μ M of Dye **1**. Spectra for dark controls were obtained after the spectra of the irradiated samples were obtained. The initial spectrum was used as a reference for any degradation that may have taken place over the course of the entire experiment..... 32
- Figure 3-8: The fluorescence emission spectrum of 200 nM quinine in 500 mM sulfuric acid used as reference for Dye **1** fluorescence in the presence and absence of CT-DNA..... 33
- Figure 3-9: The above emission spectra were obtained using a fluorimeter and the absorbance spectra were obtained using a separate spectrophotometer. (A) Low fluorescence is observed for 400 nM Dye **1** in DMSO when compared to 200 nM quinine reference in Figure 3-8. The absorbance spectrum shown as a reference consisted of 10 μ M Dye **1** in DMSO..... 34
- Figure 3-10: The CD and induced CD spectra of 20 μ M Dye **1** in the presence of 10 mM phosphate buffer pH 7.0 and 100 μ M bp CT-DNA. The absorbance spectrum sample contained 20 μ M Dye **1**, 10 mM phosphate buffer pH 7.0, and 100 μ M bp CT-DNA as well..... 36
- Figure 3-11: As the temperature conditions are decreased an obvious increase in nicked and linear forms of plasmid DNA can be observed, indicating either an indirect or direct correlation between temperature and photocleavage exists. Samples contained 38 μ M bp pUC 19, 10 mM phosphate buffer pH 7.0, and 50 μ M of Dye **1** or equal amounts of DMSO (Lanes 1, 5 and 9). 37
- Figure 3-12: This graph shows a correlation between the three temperatures used in the photocleavage experiments with yields of nicked plasmid. These temperatures were

chosen based on the different available cooling methods that provided consistent results.

..... 37

Figure 3-13: This photocleavage titration was done to show the increase in photocleavage as a function of dye concentration. Samples contained different concentrations of Dye **1** (Lanes 2-5) with 10 mM phosphate buffer pH 7.0 and 38 μM bp pUC19 with a reference containing equal amounts of DMSO (Lane 1). Samples were irradiated at 780 nm with 83 mW laser for 30 min at $-72\text{ }^{\circ}\text{C}$ 38

Figure 3-14: The initial photocleavage kinetics experiment to determine the sufficient end time for future kinetics experiments. Samples contained either 50 μM or 70 μM concentrations of Dye **1** in the presence of 10 mM phosphate buffer 7.0 and 38 μM bp pUC19. Samples were irradiated using the 83 mW 780 nm laser for 30 or 60 min at $-72\text{ }^{\circ}\text{C}$ 39

Figure 3-15: The kinetics photocleavage assay to determine the rate order of the photocleavage reaction. Samples contained 70 μM of Dye **1**, 10 mM phosphate buffer pH 7.0, and 38 μM bp pUC19. Samples were irradiated with a 780 nm 83 mW laser at $-72\text{ }^{\circ}\text{C}$ for the times listed above. 40

Figure 3-16: This graph shows the % supercoiled vs. time as a test for zero order reaction kinetics. The reactions were carried out consistently at $-72\text{ }^{\circ}\text{C}$. A 780 nm 83 mW laser was utilized for each sample. Two outliers (1 and 10 min) were removed and are not shown in the above plot. 41

Figure 3-17: This graph shows the natural log of supercoiled concentration vs. time as a test for first order reaction kinetics. The reactions were carried out consistently at $-72\text{ }^{\circ}\text{C}$. A 780 nm 83 mW laser was utilized for each sample. Two outliers (1 and 10 min) were removed and are not shown in the above plot. 41

Figure 3-18: This graph shows the reciprocal plot of supercoiled concentration vs. time which tests for second order reaction kinetics. The reactions were carried out consistently at -72 °C. A 780 nm 83 mW laser was utilized for each sample. Two outliers (1 and 10 min) have been removed to compare the most consistent cleavage yields. 42

Figure 3-19: This chart consists of the averages over three trials and standard deviations of the ROS scavenger experiments (except for KI which was done in one trial) in addition to the argon purging experiments. The argon purging enhancement was calculated by the difference of % total nicked DNA between the samples purged with air and the samples purged with argon divided by the samples purged with air. Similar calculations were done for the other scavenger experiments with the difference of % total nicked DNA without scavenger and the % total nicked DNA with scavenger divided by % total nicked DNA without scavenger. 43

Figure 3-20: The photocleavage experiment using air and argon purging to determine the role molecular oxygen plays in the photocleavage mechanism. Samples were gently purged with argon or air for 1 min. Samples containing 70 μ M Dye 1 or equal amounts of DMSO (Lane 1), 10 mM phosphate buffer pH 7.0, and 38 μ M bp pUC19 were irradiated using 780 nm 83 mW lasers for 30 min after adjusting to the appropriate temperature... 44

Figure 3-21: The photocleavage inhibition binding investigation consisted of using compounds with established DNA binding modes to inhibit photocleavage by Dye 1. The samples contained equal concentrations (70 μ M) of either methyl green (M), ethidium bromide (E), or pentamidine (P) with 70 μ M of Dye 1. The samples also contained 10 mM phosphate buffer pH 7.0 and 38 μ M bp pUC19. The samples were equilibrated for 5 min with Dye 1 first for 5 min (D + I) or with the inhibitor first for 5 min (I + D) and then

vice versa. Samples were kept at $-72\text{ }^{\circ}\text{C}$ while each were individually irradiated using an 83 mW 780 nm laser for 30 min. The other trials can be seen in the Appendix Figures 0.11-0.12)..... 45

Figure 3-22: This graph shows the percent inhibition of nicked DNA by compounds with known binding modes. These values represent averages over three trials with standard deviations shown through error bars. Order of equilibration of added compounds shown as either D + I or I + D. Abbreviations: Dye **1** (D), Inhibitor (I), methyl green (M), ethidium bromide (E), and pentamidine (P). 46

1 INTRODUCTION

1.1 Cyanine Dyes

Ever since the synthesis of the first cyanine dye by Greville Williams in 1856, and later the elucidation of the structure in 20th century, there has been a considerable amount of applications realized through the seemingly limitless customization of the compound's general structure. Cyanine dyes (CD) were not utilized in dyeing fabrics because of their innate instability in the presence of light, however, they were later found to be valuable in photographic sensitization by affording sensitivity to silver halide emulsions in other parts of the visible spectrum.¹ Recently, these synthetic dyes have been implemented in various liquid crystal displays and even more modern organic light-emitting diode displays as hi-tech applications have come to fruition.² For the past few decades, these cyanine dyes have been utilized extensively in structural biology and biochemistry as fluorescent probes and in medicine as diagnostic tools for cancer.²⁻³

The advantage of cyanine dyes in biology and medicine as fluorophores is evident in their remarkable extinction coefficients and high fluorescence quantum yields. This has fostered recent research efforts focused on expanding upon these properties by shifting the absorption spectra towards the near-infrared (NIR) region accordingly. By extending the polymethine bridge and by adding certain functional groups or atoms, the dyes' spectra can be red-shifted, therein improving upon their applications in therapeutics, and as probes and diagnostic agents. This is noteworthy because light penetration in tissue increases with longer wavelengths affording a more effective means of treatment and/or diagnostics.⁴

1.1.1 General Structure and Modifications

The core structure of cyanine dyes consists of two nitrogen centers, often within heterocyclic rings, connected by a conjugated polymethine bridge with an odd number of carbons. One of the

nitrogen atoms is positively charged, inducing what is known as a “push-pull” mechanism of resonance within the polymethine system of the chromophore between the quaternary nitrogen and the donating nitrogen atom. This conjugated system is the underpinning moiety of the chromophore, generating the characteristic cyanine $\pi\pi^*$ transition which can be extended into the NIR region by approximately 100 nm for every additional vinyl group in the polymethine bridge. A general structure of symmetrical heterocyclic cyanine dyes can be seen in Figure 1-1 below.

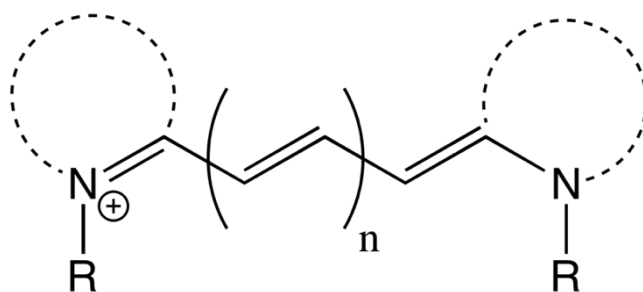
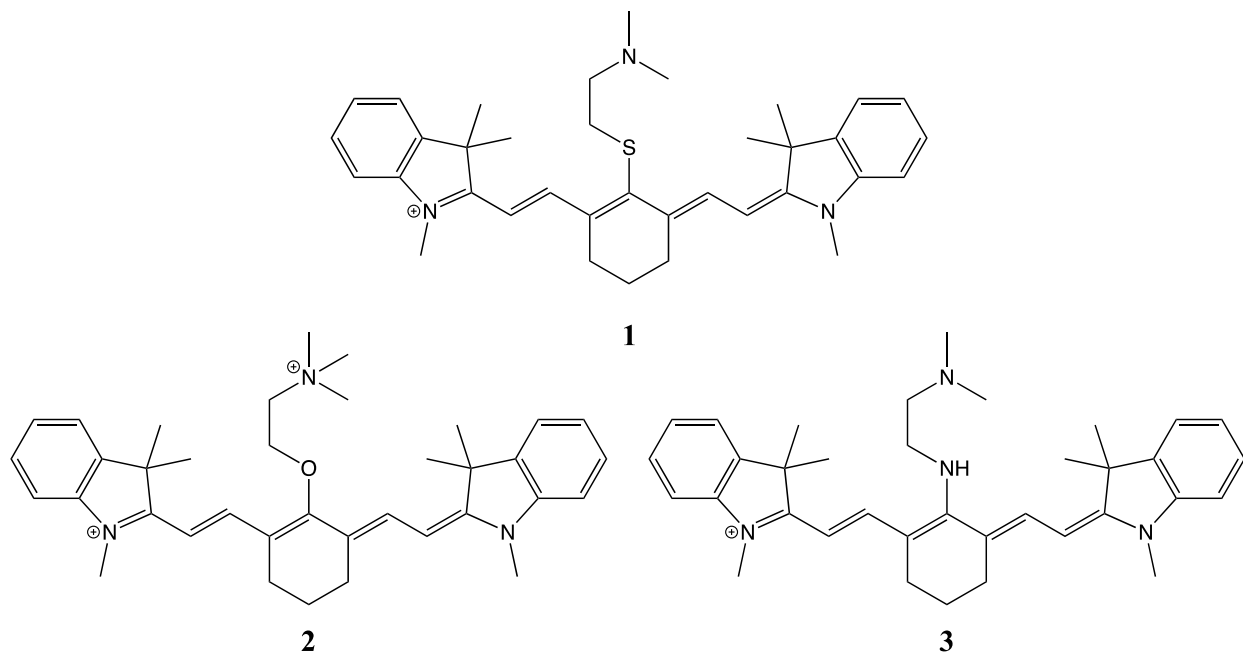


Figure 1-1: General structure of symmetrical cyanine dyes.

Heptamethine cyanine dyes have a polymethine bridge consisting of 7 carbons and have strongly influenced the fields of fluorescence microscopy and diagnostics with novel compounds such as indocyanine green, Cy5.5, and IRDye800-C.³ Unfortunately, the length of the polymethine bridge reduces stability and rigidity with every additional vinyl group. However, it has been shown that including a cyclohexenyl ring at the center of the bridge increases rigidity and stability while also improving upon the fluorescence quantum yield. It was determined that a nonamethine cyanine without stabilizing cyclohexenyl rings degraded 70% within 45 min whereas a bridged nonamethine cyanine with cyclohexenyl rings showed 5% decomposition after 24 h.⁵ Additionally, various heterocyclic ring structures have been shown to influence dye aggregation and degradation in various solvents as well as in the presence of certain biomolecules.

Several ring systems including pyridine, quinoline, indolium, benzothiole, and benoxazole have been incorporated into cyanine dyes and can contribute to the resonance delocalization afforded by the methine linker.⁶ One focus of current synthetic efforts in regards to developing better fluorophores and photosensitizers has been to improve photostability by increasing rigidity. An additional effect of rigidity is to limit internal conversion (IC), a competing energy pathway which decreases the fluorescence and triplet state quantum yields.⁵ In this thesis, the heptamethine cyanine dyes below are spectroscopically compared with Dye **1** (containing a meso-substituted captamine) being further investigated. Dyes **1-3**, seen in Figure 1-2 below, are symmetrical with indolium ring systems on both sides of the polymethine bridge. By only changing the central electron donating group, this provides an elegant spectroscopic comparison in regards to developing efficient NIR photosensitizers.



*Figure 1-2: The structures of the cyanine dyes that are compared and investigated in this paper. Dyes **1** and **3** were synthesized by Xiaozhong Ma and Dye **2** was synthesized by Andy Levitz, under the direction of Dr. Maged Henary.*

1.1.2 Aggregation

Certain aggregation states or nanoclusters can strongly affect the luminescent properties of cyanine dyes. Various arrangements can occur based on the polarity of the solvent, temperature, concentration, pH, and ionic strength. Due to their highly conjugated structures, cyanine dyes self-aggregate via van der Waals-induced π - π stacking. This stacking phenomenon can result in J-aggregation or H-aggregation producing a bathochromic or hypsochromic shift in the spectra, respectively. The aggregation state is determined by the angle of slippage between consecutive dyes with J-aggregates forming due to a larger angle and H-aggregates forming due to a smaller angle.⁶⁻⁷ At low concentrations, certain monomeric cyanine dyes tend to bind readily to DNA. However, as the concentration of dye is increased, cyanines can begin to bind to DNA as aggregates.⁷

1.1.3 DNA Binding and Interaction

Cyanine dyes have been shown to interact with DNA in various ways that have been attributed to their aromatic ring systems, delocalized positive charge, and aggregating properties.⁸ Intercalation between the base pairs occurs if a sufficient heterocyclic ring system can participate in π - π stacking interactions facilitated by resonance within the aromatic rings. This mode of binding has been particularly advantageous in developing cyanine dyes that fluoresce at high intensities upon intercalation.⁹ Certain bent-shaped symmetrical cyanine dyes have been shown to exhibit sequence-specific DNA recognition through minor groove binding.¹⁰ While hydrophobic interactions have been shown to elicit minor groove binding electrostatic interactions between the negatively charged phosphodiester groups and the delocalized positive charge on the polymethine bridge has been shown to be an alternative mode of interaction.¹¹

1.2 Photosensitizers

Photosensitizers (PS) are molecules that absorb light and can be transitioned to the excited triplet state via intersystem crossing (ISC) from the excited singlet state. Upon absorbance of a photon of a particular energy, an ideal photosensitizer will exhibit ISC by inversion of an electron spin, allowing for a longer excited energy lifetime in the triplet state. The longer lifetime of the triplet state provides more time for sufficient interaction with triplet ground state oxygen resulting in one or two types of photochemical pathways. A Type I reaction occurs if an electron is transferred directly to ground state triplet oxygen from the PS which can result in the formation of reactive oxygen species through Fenton-like chemistry. Type II energy transfer occurs if the PS transfers energy directly to molecular oxygen through a collision resulting in a singlet ground state PS and a highly reactive singlet oxygen.^{4, 12-15} An efficient PS will be characterized by low fluorescence quantum yields, higher rates of ISC, and high triplet state quantum yields and lifetimes. Additionally, limiting internal conversion through improved molecular rigidity is typical of an ideal PS.⁵ The general overview of the various photochemical processes that can occur once a PS absorbs light can be seen in Figure 3-3 below.

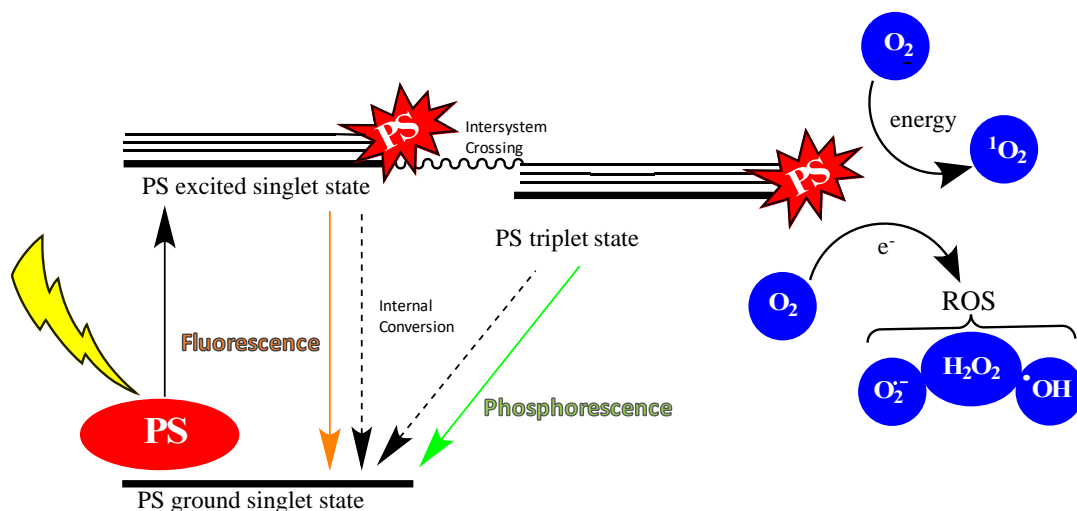


Figure 1-3: This illustrates the Jablonski diagram in relation to generating reactive oxygen species through Type I and Type II energy transfer pathways. Nonradiative pathways (intersystem crossing and internal conversion) are also shown.

Tetrapyrroles are currently the most common structures found in photosensitizers in regards to cancer treatment and are ubiquitous in many relevant biomolecules (*e.g.* chlorophyll, haem, bacteriochlorophyll).⁴ One example of an FDA approved PS that utilizes the tetrapyrrole moiety is Photofrin® which can be used to treat reoccurring breast cancer on the chest wall.¹⁶ Recent research efforts have been made in developing synthetic dyes as photosensitizers with applications in photodynamic therapy (PDT). Towards this end, cyanine dyes and squaraine dyes exhibit remarkable molar absorptivity and can be easily purified. Synthetic dyes show potential in addressing current limitations in photodynamic therapy such as issues with internalization, specificity, and absorbing light within the therapeutic window.³⁻⁴ Certain fluorescent heptamethine cyanine dyes have shown preferential tumor uptake while also absorbing near-infrared light.¹⁷ This indicates that an auspicious prospect may exist in developing ideal PSs by adjusting cyanine dye fluorophores with preferential tumor internalization to act instead as photosensitizing agents.

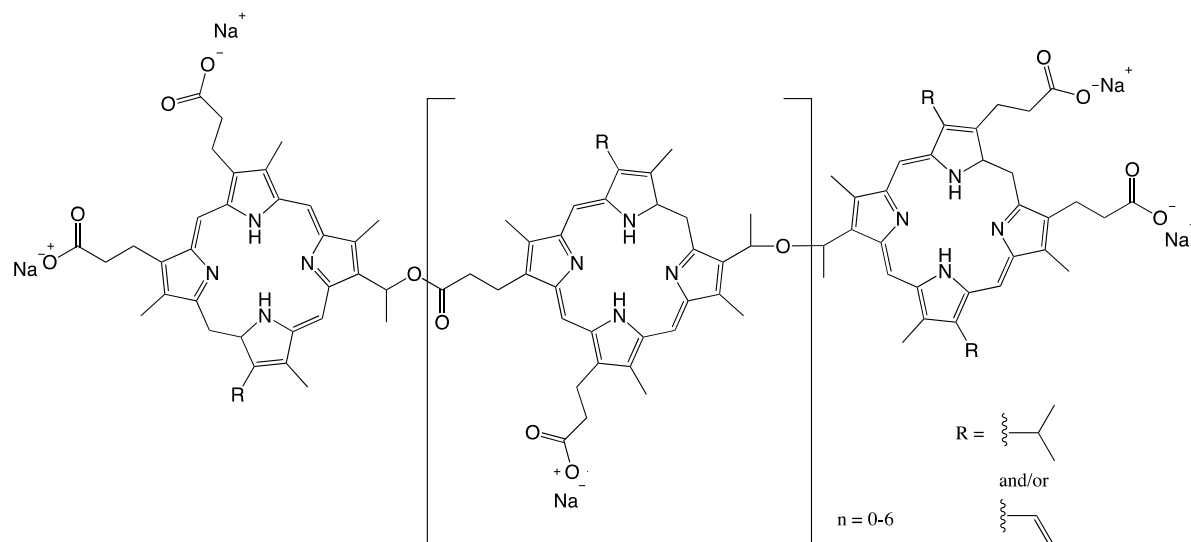


Figure 1-4: The structure of profimer sodium (Photofrin®), a current FDA approved photosensitizer that absorbs red light.

1.2.1 Photodynamic Therapy

Photodynamic therapy consists of administering a non-toxic PS through systematic means or directly into the area that needs treatment. After equilibration and incubation, the PS is selectively activated with light of an appropriate wavelength using lasers, fiber optics, or medical lamps. PDT represents a promising form of cancer treatment as it seeks to address specificity and selectivity between healthy and cancerous tissues. As mentioned previously, a current limitation on PDT is poor tissue penetration by UV and visible light, therefore, recent research efforts have concentrated on developing NIR absorbing agents within the “therapeutic window”, the region of the electromagnetic spectrum between 700 and 900 nm with optimal light penetration between 800 and 900 nm.¹¹⁻¹⁶

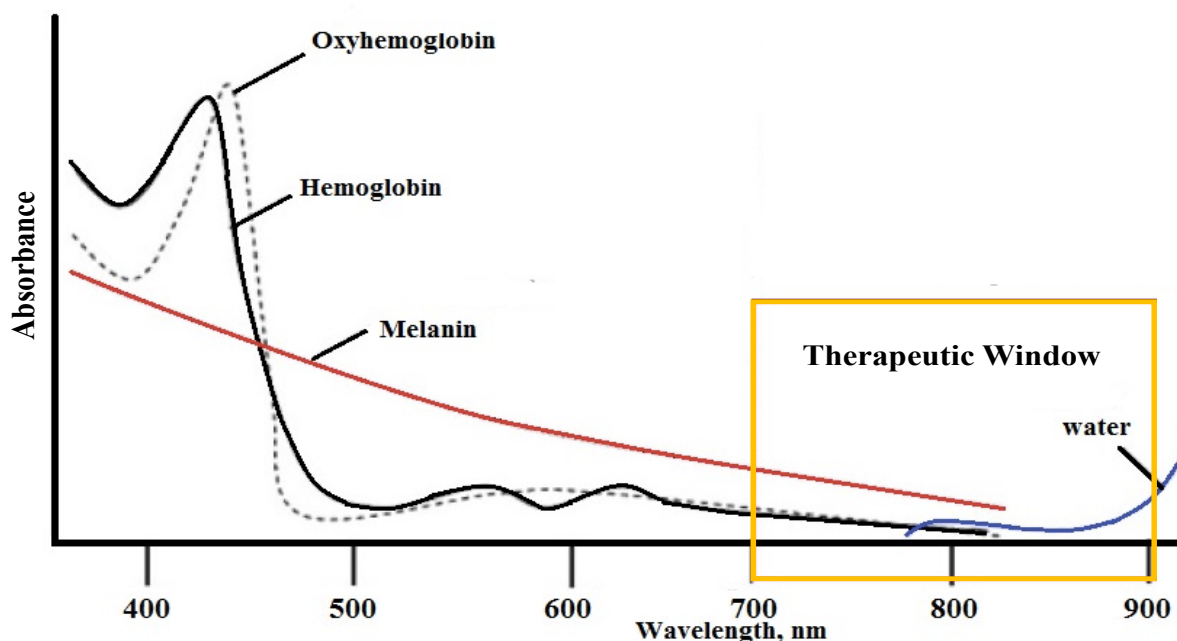


Figure 1-5: The box illustrates the absorption region that represents the PDT therapeutic window. This is located between absorption by ubiquitous biomolecules (UV/visible region) and water, which absorbs in the infrared region.¹⁴

1.2.2 Reactive Oxygen Species

Oxygen is a necessary component of PDT for the vast majority of photosensitizing agents. The reactive oxygen species (ROS), hydroxyl radicals, hydrogen peroxide, singlet oxygen, and superoxide anion radicals, are directly and indirectly responsible for the biomolecular cleavages which result in disruption of cellular functions and ultimately lead to cell death through apoptosis or necrosis. The diffusion differences of the most powerful ROS, hydroxyl radicals and singlet oxygen, are highly limited due to their instability and presence of cellular antioxidants, therefore, PSs with a particular binding affinity for vital biomolecules and organelles are favorable and can increase specificity.^{4, 12-16}

1.2.3 Advantages of Sulfur-substituted Photosensitizers

1.2.3.1 Increased Intersystem Crossing Rate

Recently, Peceli et al. showed that sulfur-substituted polymethine dyes (PDs) when compared to oxygen-substituted analogues dramatically enhanced intersystem crossing rates. This was particularly attributed to the transposition of the lowest energy $\pi\pi^*$ transition relative to the $n\pi^*$ state which leads to a diminished energy gap between the singlet and triplet states. This inversion has three effective augmentations on the spin-orbital coupling Hamiltonian (H_{SOC}), ergo decreasing the inhibitive singlet-triplet energy gap that prevents triplet state formation.¹⁸⁻¹⁹ In their paper, the authors describe the increased efficacy of the spin-orbit coupling as being caused by the integration of singlet and triplet states belonging to different molecular orbital configurations as expressed by the El-Sayed rule.^{18, 20} Specifically, this rule characterizes increased intersystem crossing rates, attributing enhancements to the conversion of molecular orbitals of different types in the radiationless transition. Experimentally, El-Sayed found an increase in k_{ST} of up to 1000 times that of transitions between two states of the same electronic basis such as $\pi\pi^*$ to $\pi\pi^*$ transitions.²⁰

The inversion also induces a reduced energy gap between the singlet and triplet states facilitating the transition process. Additionally, the dark electronic singlet state (n,π^*) has a prolonged radiative lifetime, resulting in a directed nonradiative transition via intersystem crossing. Peceli et al. also showed that when compared to the enhancement in intersystem crossing exhibited by the sulfur-substituted PDs, the dyes designed to employ the heavy-atom effect had insignificant triplet quantum yields.¹⁸ The results suggest that incorporating sulfur containing substituents may be the superior way to increasing the triplet state yield through uniform radiationless intersystem crossing.

1.2.3.2 Sulfur Radicals and Tumor Hypoxia

Tumor hypoxia, or the lack of oxygen in certain cancers, was suspected for decades and confirmed in the 1990s with the advent of oxygen electrodes allowing for precise measurements of oxygen levels. Results indicated that oxygen levels in solid tumors were vastly heterogeneous with cells farther away from blood vessels receiving less oxygen. Since oxygen is a requisite in many forms of cancer treatment such as radiotherapy, evidence reveals that oxygen-dependent cancer treatments decrease in efficacy in oxygen-starved areas of tumors.²¹ Additionally, analyses show that hypoxia is a contributing feature of tumor progression with an increase in cell division observed in higher levels of hypoxia.²² As a result, a rise in research efforts is occurring aimed at addressing this limitation in current therapeutics and the development of synthetic compounds that can be used in photodynamic therapy in both aerobic and anaerobic tumor environments.²³⁻²⁴ An illustration of the necessary higher doses of radiation for hypoxic cells can be seen below in Figure 1-6.

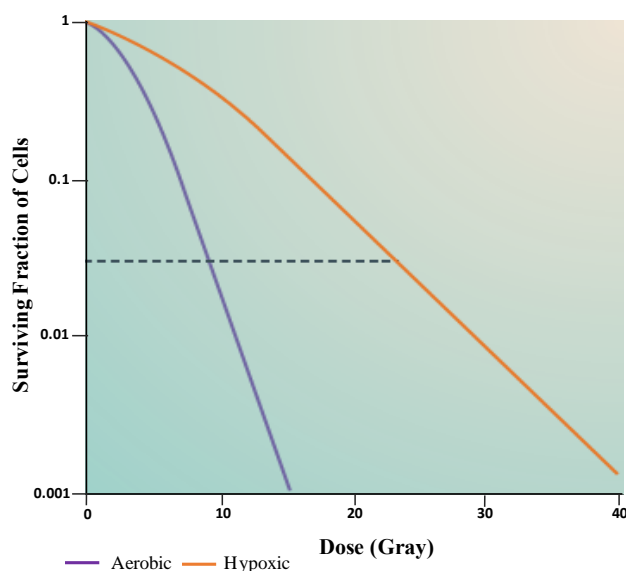


Figure 1-6: This graph shows the cell-survival curves for both hypoxic and aerobic cells receiving radiosensitizer doses that result in the same fraction of surviving cells. Higher doses are needed for hypoxic cells due to the lack of available oxygen.²¹ The SI unit Gy (Gray) is equivalent to the absorption of one joule of radiation energy per kg.

In addition to ROS and reactive nitrogen species (RNS), there is evidence that reactive sulfur species (RSS) play a role in physiochemical processes, specifically in the neutralization of antioxidant radicals containing thiols such as glutathione.²⁵ Sulfur-centered radical cations have garnered attention in organic synthesis as dialkyl sulfur radicals and aromatic sulfides in aqueous solutions sensitized by pulse radiolysis in the presence of oxidizing species.²⁶⁻²⁷ Wauchope et al. showed that sulfur-incorporated dibenzothiophene S-oxide can photocleave DNA under anaerobic conditions, providing further evidence that sulfur organic compounds can potentially participate in light-induced radical cleavage mechanisms without the involvement of oxygen.²⁴ Furthermore, certain metal-containing photosensitizers have been shown to photocleave DNA in argon-purged solutions representing a significant stride in developing oxygen-independent phototherapeutics.²³ Given the inherent issues regarding tumor hypoxia and oxygen-dependent therapeutics, sulfur-based agents that participate in oxygen-independent photo-induced DNA cleavage present a promising path forward in the development of photosensitizing agents in PDT.

1.3 Low-Temperature Effects

From the excited singlet state, there are several general outcomes when energy is absorbed in the form of light by a molecule: the energy is emitted in the form of fluorescence at a longer wavelength, translated to heat via vibrational relaxation, or a spin-forbidden transition to the triplet state can occur which can result in phosphorescence or triplet state energy transfer.²⁸ The effects of temperature on photochemical reactions has been investigated and conjectured for decades with nuances between nonradiative transitions and radiative transitions being probed by numerous experiments. Radiative transitions rates (i.e. fluorescence or phosphorescence) have

been shown to be largely unaffected by temperature, however, quantum yields and state lifetimes have been shown to vary with temperature in certain instances. This implies that radiationless processes may be influenced by temperature if higher vibrational levels in the excited state result in different photochemistry when compared to $v = 0$.¹⁹ In Figure 1-7, the competitive nature of potential photochemical reactions at various vibrational states is illustrated with respect to nonradiative relaxation and fluorescence from the lowest energy vibrational state.

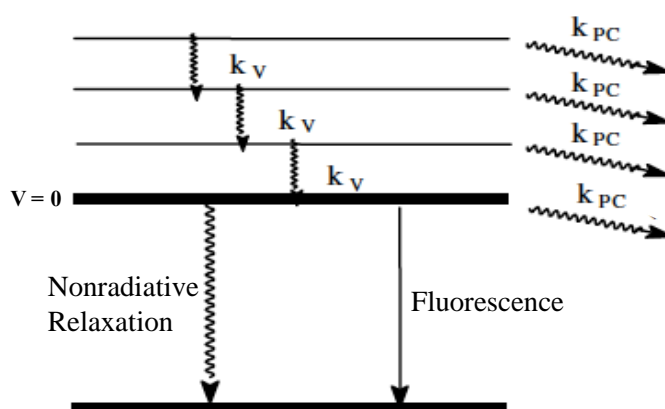


Figure 1-7: This form of the Jablonski diagram illustrates the competitive pathway of vibrational relaxation through internal conversion in regards to other photochemical processes. Abbreviations: k_v stands for the vibrational relaxation or internal conversion rate constant, k_{PC} stands for the photochemistry rate constant.²⁹

1.3.1 Temperature Effects on Nonradiative Processes

As mentioned previously, internal and external conversions (IC and EC) are inhibiting pathways when fluorophores or photosensitizers are excited to higher energy states. Internal conversion proceeds when electronic energy is translated into vibrational energy and rotational energy whereas external conversion concerns the loss of electronic energy through solvent and solute collisions. Internal conversion in the form of S_1 to S_0 deactivation is poorly understood, however, the rate of internal conversion from S_n to S_1 is approximately 10^6 greater than that of

the S_1 to S_0 deactivation for a series of aromatic hydrocarbons. When compared to much higher rate constants of radiative deactivation, the contribution of internal conversion to excited state depopulation is considerably negligible.¹⁹ However, vibronic deactivation in the form of internal and external conversion is propelled by thermal processes, therefore, lowering the temperature of photochemical processes can inhibit these pathways from competing with radiative processes or intersystem crossing.²⁸⁻²⁹

Intersystem crossing has been shown to be temperature dependent for certain molecular species with an increase in k_{ST} (intersystem crossing rate) as temperature is decreased, however, the reasoning behind the enhancement has been largely studied in the context of solid matrices and solvent effects.³⁰ Meyer et al showed that the increased k_{ST} for SO_2 in a low-temperature solid solution with limited solvent interactions was notable when compared to k_F or k_{IC} , suggesting a robust temperature correlation. Conversely, Song and Fayer determined a thermally activated k_{ST} for rubrene in a solid state solution where no intersystem crossing is observed at room temperature.³¹ An important distinction is the absorption of another photon in the excited triplet state which is above the reported range associated with the T_1 state, indicating an S_1 or T_1 to $T_{n>1}$ transition.³¹ This implies that intersystem crossing to higher energy, dark triplet states can be thermally activated whereas phosphorescence upon a S_1 to T_1 transition can be amplified at lower temperatures.

A temperature effect has also been shown to exist for phosphorescence lifetimes of different aromatic hydrocarbons.³²⁻³³ Additionally, Kellogg and Schwenker showed that the triplet state lifetimes for a series of aromatic hydrocarbons were increased at lower temperatures, however, this was minimal with an increase in the triplet state lifetime by a factor of less than two from 300 K to 4 K.^{19, 33} The temperature range used in the procedures presented in this thesis range

from 298 K to 201 K, indicating little to no temperature effect on the triplet state lifetime of Dye **1** should be observed.

1.3.2 Temperature Effects on Photobleaching

Photobleaching has been studied extensively in the field of fluorescence microscopy as well as in developing more stable photosensitizers, however, research efforts to reduce photobleaching and understand the pathways involved have remained a vital component in developing better therapeutics and diagnostics. Photobleaching, also known as photofading or dye photolysis, involves photochemical changes (*e.g.* photooxidation, intramolecular reactions, photoisomerization, or reactions between adjacent compounds) to the dye which permanently inhibits its function.³⁴ Photostability, oxygen levels, light intensity, excitation time, and other factors play a role in photobleaching pathways.³⁴ Although lowering the molecular oxygen levels in samples and increasing photostability of fluorophores has assisted in improving fluorescence microscopy and imaging, photosensitizers have been largely restricted to improvements on photostability because of the necessity of oxygen in most photosensitizing processes.

Although photooxidation significantly contributes to the overall bleaching effect at room temperature, the diffusion constant and permeability of a solid matrix in regards to solubility of oxygen may play a role at lower temperatures.³⁵ The solvent and temperature dependent mobility of oxygen and molecules in general is associated with the rotational and translational energy of the solvent. Temperature effects on photobleaching have been attributed to differences in activation energy barriers of photochemical reactions which implies that lower temperatures can decrease photobleaching phenomena for certain molecular species.³⁶⁻³⁷ Furthermore, the restricted diffusion of water and other reactive species such as ROS may contribute to a decrease in photobleaching at lower temperatures.³⁵ It has been observed that photobleaching of

Rhodamine 6G in a poly(vinyl alcohol) matrix was drastically reduced when the temperature was decreased from 295 to 200 K. Additionally, when water is present it has been shown to increase oxygen dissemination in the PVA matrix also affecting the overall rigidity of the molecule. This was in agreement with previous indications that water is involved in the photobleaching process, however, Zondervan et al. observed photobleaching at 10 K demonstrating that some photolysis mechanisms persist with little to no energy barrier.³⁵

1.4 Summary of Research

The purpose for the research described in this thesis is to explain two phenomena: the remarkable enhancement in photocleavage of pUC19 DNA by a sulfur-based cyanine dye when the temperature is lowered and the advantageous properties of sulfur incorporation into photosensitizing agents. The cyanines synthesized by Dr. Maged Henary's lab at Georgia State University allowed for a facile comparison of the spectroscopic effects attributed to sulfur via UV-visible and fluorescence spectroscopies. The stability of the DNA-dye complex was then confirmed and CD spectroscopy was employed to provide further evidence for DNA-dye interaction. Through obtained UV-visible spectra, it was determined that GaAlAs semiconductor lasers (780 nm irradiation) were the most suitable to conduct the photocleavage experiments. Scavenger assays were carried out to identify the reactive oxygen species involved in the DNA photocleavage. Additionally, elevated DNA cleavage yields obtained upon purging with argon indicated an alternative oxygen-independent cleavage mechanism might exist for certain sulfur-substituted photosensitizers.

2 EXPERIMENT

2.1 Materials and Instrumentation

Cyanine Dyes **1** and **3** were synthesized and purified by Xiaozhong Ma and Dye **2** was synthesized and purified by Andy Levitz in Dr. Maged Henary's Lab (Georgia State University). All dyes were dissolved in dimethyl sulfoxide (DMSO) purchased from Sigma-Aldrich (St. Louis, MO). UltraPure™ Calf thymus DNA was obtained from Invitrogen (Cat. No. 15633019, Lot No. 780948) and quantitated using a PerkinElmer Lambda 35 UV/VIS spectrophotometer. All pUC19 DNA was kept in sodium phosphate buffer (pH 7.0) and prepared by transfecting *E. coli* via artificial competence by heat shock (Stratagene, XL-1 blue). The transfected cells were cloned in bacterial cultures and purified using the QIAfilter Plasmid Mega Kit (Qiagen™, Cat no. 12263). Agarose was purchased from either BioRad (Herclues, CA), Fischer Scientific (Fairlawn, NJ), or Research Products International (Mt. Prospect, IL). Ethidium bromide (EtBr) and methanol ($\geq 99.8\%$) were from Sigma-Aldrich (St. Louis, MO). For binding mode studies, methyl green was purchased from GTI Laboratories Supplies (Houston, TX) and pentamidine isethionate salt was purchased from Sigma-Aldrich (St. Louis, MO).

Water was deionized using an AQUA SOLUTIONS® Type 1 DI System (Jasper, GA) and all experiments utilized sodium phosphate buffer (pH 7.0) prepared from monobasic and dibasic sodium phosphate from Fischer Scientific (Fairlawn, NJ). The prepared tris base, acetic acid, and EDTA buffer (TAE buffer) was prepared using ethylenediaminetetraacetic acid disodium salt (EDTA) purchased from IBI Scientific (Peosta, IA) and tris(hydroxymethyl)aminomethane from Research Product International (Mt. Prospect, IL). Scavenger experiments were done using D₂O (99%) and sodium benzoate (99%) purchased from Sigma-Aldrich (St. Louis, MO) as well as

EDTA purchased from IBI Scientific (Peosta, IA). Ultra-high purity argon gas was distributed by NexAir (Memphis, TN).

Dye **1** was irradiated with GaAlAs semiconductor lasers (maximum optical output at 780 nm between 69 to 83 mW) which were purchased from Laser Land Company. The UV-Visible spectra were recorded using the PerkinElmer Lambda 35 UV/VIS and all fluorescence spectra were acquired using an RF-1501 spectrofluorometer from Shimadzu Scientific Instruments. The circular dichroism (CD) and induced circular dichroism (ICD) spectra were obtained using a Jasco J-810 spectropolarimeter. Gel Electrophoresis was done using a Wide Mini-Sub Cell® BioRad Gel Box with an applied constant voltage of approximately 100 V. A GIBCO BRL power supply unit from Life Technologies was used to apply an electric field. All gels were visualized using the VWR Scientific LM-20E transilluminator (302 nm) and photographed with a UVP PhotoDoc-It™ imaging system. Gel quantitation was done using ImageQuant version 5.2 program and Microsoft Excel. Temperatures were recorded using a Toluene-based Ultra Low Liquid-in-Glass Thermometer from DURAC® Plus™ (Trappe, PA).

2.2 Methods

2.2.1 UV-Visible Spectrophotometry

All absorbance spectra were recorded from the IR region (1100 nm) through the UV region (200 nm) to determine aggregation and stability of the dyes over time. The time courses were done in increments of five min for a total time span of 30 min resulting in 7 separate spectra. The absorbance spectra were recorded in DMSO at a concentration of 10 μ M for each dye.

Absorbance spectra for Dyes **1** and **3** were also acquired in a 10 mM aqueous sodium phosphate buffer solution at pH 7.0 to determine stability in the absence of DNA. Absorbance spectra for

Dyes **1** and **3** were then recorded in the presence of 150 μM bp CT-DNA in 10 mM aqueous sodium phosphate buffer (pH 7.0). The Dye-DNA complex spectra were then used to determine the optimum irradiation wavelength for photocleavage experiments and to determine stability of the dyes in the presence of DNA. Dye **2** was only recorded in DMSO so that spectroscopic features could be compared with Dye **1** based on the sulfur and oxygen substitution.

2.2.1.1 DNA Titration

A CT-DNA titration was done to determine the optimum concentration for observing induced CD signals (ICD). A 10 μM initial concentration of Dye **1** in 10 mM phosphate buffer was recorded before 1 μL increments of $1.49 \times 10^3 \mu\text{M}$ bp CT-DNA were added directly to the quartz cuvette. A spectrum was then acquired after each addition of CT-DNA and the titration was carried out until the dye was completely saturated with no observed difference between consecutive spectra. An additional titration was done using a 20 μM concentration of Dye **1** after observing an improved ICD signal after doubling the dye concentration. It was then determined that a 20 μM concentration of Dye with 60 μM bp CT-DNA was optimal for observing an ICD signal around 700 nm.

2.2.1.2 Temperature Effects on Aggregation

Since dye aggregation can affect the propensity for photocleavage, temperature effects on aggregation were considered. A 4.2 mL solution of 10 mM phosphate buffer, 60 μM bp CT-DNA, and 5 μM of Dye **1** was separated out into 600 μL aliquots for a total of three aliquots at room temperature and four aliquots at 2 $^{\circ}\text{C}$. The spectra at room temperature (24 $^{\circ}\text{C}$) were immediately and consecutively obtained by adding 500 μL of each sample to the quartz cuvette. The other four samples were subjected to colder temperatures using metal blocks surrounded either in ice with sodium chloride (4 samples at 2 $^{\circ}\text{C}$) for at least 10 min. The spectra of the

colder solutions in saline/ice conditions were then immediately and consecutively obtained after the allotted 10 min by adding 500 μL of each sample to the quartz cuvette.

2.2.1.3 Temperature Effects on Photobleaching

A 1 mL working stock containing 10 mM phosphate buffer, 150 μM bp CT-DNA, and 10 μM of Dye **1** was separated into 60 μL aliquots. Initial spectra were immediately taken by adding 50 μL of the samples into 450 μL of dH_2O in a quartz cuvette. Two aliquots were then subjected to dry ice conditions ($-72\text{ }^\circ\text{C}$) for 5 min before being irradiated using an 83 mW 780 nm laser. Both samples were irradiated for 3 min and then slowly brought to room temperature before transferring 50 μL into a cuvette containing 450 μL of dH_2O . Two more aliquots were irradiated as previously described but at $24\text{ }^\circ\text{C}$ and then likewise diluted into a cuvette. The spectra of the dark controls for each temperature were then recorded so that any change in absorption spectra were attributed to irradiation.

2.2.2 Circular Dichroism

Circular Dichroism (CD) is often employed to study interactions between achiral ligands and DNA. Since DNA is chiral, an achiral dye induced CD (ICD) signal can be observed in the CD spectrum if interactions with DNA are present.³⁸ As previously described, the optimized DNA and dye concentrations were determined by UV-visible spectrophotometry to evaluate the apparent binding mode. The samples were prepared in a 3 mL quartz cuvette with a 1 cm path length as described by Garbett et al. for the analysis of weak ICD signals.³⁸

First, a 1.5 mL phosphate buffer solution pH 7.0 at a concentration of 10 mM was prepared and the spectrum was recorded. The spectrum was then used to subtract any potential

absorbance contributions made by the buffer. Two separate 1.5 mL samples containing 10 μM Dye **1** in a 10 mM phosphate buffer solution and a 100 μM bp CT-DNA and 10 mM phosphate buffer solution were prepared and their spectra recorded. A final solution containing 20 μM of Dye **1**, 100 μM bp CT-DNA, and 10 mM phosphate buffer was left to equilibrate for 1 min and a spectrum was then recorded. All data were obtained over 12 accumulations using the following parameters: 0.5 nm pitch, 1 nm bandwidth, and a 2 s response time with a scanning speed of 200 nm/min. Additionally, for all samples the sensitivity of the detector was set to 100 mdeg and spectra were recorded from 900 to 200 nm.

2.2.3 Fluorescence Spectroscopy

Cyanine dyes have been known to exhibit fluorescence in the presence and absence of DNA.^{3,8,17} Although Peceli et al. have shown that various sulfur PD analogs exhibit poor fluorescence due to fast intersystem crossing rates, fluorescence spectra of Dye **1** in DMSO as well as in the presence and absence of DNA were obtained. A 400 nM concentration of Dye **1** in a total 3 mL DMSO solution was prepared in a quartz cuvette. The excitation wavelength was set at 770 nm and the emission spectrum was recorded from 785 nm to 900 nm. In a quartz cuvette, a 2.5 mL solution of 10 mM phosphate buffer and 10 mM EDTA was prepared with 500 nM of Dye **1**. The initial concentration of CT-DNA was 0.5 μM bp and then raised in 0.5 μM bp increments to an end concentration of 2.5 μM bp. The excitation wavelength used was 715 nm and the emission spectrum was recorded from 715 nm to 850 nm.

2.2.4 Gel Electrophoresis

All gel electrophoresis was done in 1.3-1.5% agarose gels by dissolving approximately 1.5 g of agarose in a 100 mL TAE buffer (pH 7.0). The resulting agarose solution was boiled in a microwave oven until homogenous and then 10 μL of a 5 $\mu\text{g/mL}$ EtBr was added before pouring

the agarose into a gel tray and letting it sit for one hr. To each sample, 3 μL of loading buffer (15.0% (w/v) ficoll and 0.025% (w/v) bromophenol blue) was added before briefly centrifuging in a benchtop mini-centrifuge for approximately 2 s and allowing to equilibrate for 2 min. Finally, 20 μL aliquots were added to each well of the cast gel and an electric field (100 V) was applied for one hr to induce separation based on size and shape of the different forms of plasmid.

2.2.4.1 DNA Photocleavage Concentration Titration

A titration assay was performed to determine the adequate dye concentrations for sufficient DNA photocleavage at different temperatures for every batch of plasmid that was made. Reactions were prepared as described above but with 25 μM , 50 μM , 75 μM , and 100 μM concentrations of Dye 1 as shown in Table 2.1. The solutions were equilibrated for 1 min at room temperature before being added to a $-72\text{ }^\circ\text{C}$ metal block surrounded with crushed dry ice. Each sample was separately irradiated in the block for 30 min using an 83 mW 780 nm laser after adjusting all samples to $-72\text{ }^\circ\text{C}$ for 5 min. The different forms of plasmid were then electrophoresed on agarose gels.

Table 2.1: Photocleavage concentration titration was prepared with the below concentrations of Dye 1.

| | | | | |
|---------------------------------------|----|----|----|-----|
| pUC19 | + | + | + | + |
| Dye (μM) | 25 | 50 | 75 | 100 |
| Light | + | + | + | + |

?

2.2.4.2 Photocleavage Time Course Assays

Two separate photocleavage time course experiments were completed to gather preliminary kinetics data and to determine the appropriate irradiation times for subsequent scavenger experiments. The irradiation times were optimized over the course of several trials. The first trial consisted of preparing four samples containing 38 μM bp pUC19 and 10 mM

phosphate buffer with two of the samples containing 50 μM Dye **1** and the other two containing 70 μM Dye (Table 2.2). The 70 μM concentration was used based on a previous photocleavage titration with this particular batch of plasmid. The two different concentrations of Dye **1** were irradiated for 30 min and 60 min to determine the necessary end time for kinetics experiments. For the second experiment, a total of 12 samples was aliquoted out from a 480 μL solution containing 38 μM bp pUC19, 10 mM phosphate buffer, and 70 μM Dye **1** as shown in Table 2.2. One aliquot was used as a dark control and two samples without Dye **1** were used as negative light and dark controls. All solutions were kept in a metal block surrounded in crushed dry ice while each sample was being individually irradiated using an 83 mW 780 nm LED laser. The samples were adjusted to $-72\text{ }^{\circ}\text{C}$ before irradiation and were left at $10\text{ }^{\circ}\text{C}$ after irradiation while other samples were being processed. The different forms of plasmid were then separated out via gel electrophoresis.

Table 2.2: The first experiment used to optimize concentration and irradiation times for the preliminary kinetics experiments.

| | | | | |
|---------------------------------------|----|----|----|----|
| pUC19 | + | + | + | + |
| Dye (μM) | 50 | 50 | 70 | 70 |
| Time (min) | 30 | 60 | 30 | 60 |
| Light | + | + | + | + |

?

Table 2.3: The initial kinetics experiment was set up with the following times and controls.

| | | | | | | | | | | | | | |
|-------------------|---|---|---|---|---|---|----|----|----|----|----|----|----|
| pUC19 | + | + | + | + | + | + | + | + | + | + | + | + | + |
| Dye | + | + | + | + | + | + | + | + | + | + | - | + | - |
| Time (min) | 1 | 2 | 3 | 4 | 6 | 8 | 10 | 15 | 20 | 30 | 30 | 30 | 30 |
| Light | + | + | + | + | + | + | + | + | + | + | + | - | - |

?

2.2.4.3 Photocleavage with Decreasing Temperature

A total of four separate trials using three different temperatures (24 °C, 0 °C, and -72 °C) were used to evaluate DNA photocleavage by Dye 1. A total of 9 aliquots of 38 µM bp plasmid DNA, 50 µM of Dye 1, and 10 mM phosphate buffer were prepared for each trial as shown in Table 2.4. Three aliquots were used for the three available 780 nm lasers with different optical outputs (69 mW, 80 mW, and 83 mW) under the different temperatures. The total time of irradiation was 1 hr and 30 min because this experiment was done before irradiation times had been adjusted. A reference for each temperature without Dye 1 was used to measure any temperature-induced cleavage without irradiation that had occurred. A separate assay for darks controls was done using the same parameters and concentrations to show any cleavage that occurred was only done due to irradiation of Dye 1.

Table 2.2: The setup for the four trials of the photocleavage with decreasing temperatures experiment using Dye 1 can be seen below.

| | | | | | | | | | | | | |
|-------------------------|----|----|----|----|----|----|----|----|-----|-----|-----|-----|
| pUC19 | + | + | + | + | + | + | + | + | + | + | + | + |
| Dye | - | + | + | + | - | + | + | + | - | + | + | + |
| Temperature (°C) | 24 | 24 | 24 | 24 | 0 | 0 | 0 | 0 | -72 | -72 | -72 | -72 |
| Output (mW) | 69 | 69 | 80 | 83 | 69 | 69 | 80 | 83 | 69 | 69 | 80 | 83 |

?

2.2.4.4 Scavenger Experiments

ROS scavenger experiments are performed to identify the relevant reactive oxygen species involved in the DNA photocleavage mechanism. Samples were prepared with 10 mM phosphate buffer pH 7.0, 50 µM of Dye 1, and 38 µM bp of pUC19 plasmid DNA and the suitable final concentrations of scavengers. This includes 100 mM sodium azide, 100 mM EDTA, 100 mM sodium benzoate, and 75% D₂O solutions. After Dye 1 was pre-equilibrated with pUC19 for 1 min in phosphate buffer solution, the scavenger was added and further equilibrated for another 10 min at room temperature. The other samples were kept refrigerated at

10 °C while each was irradiated with an 83 mW 780 nm LED laser at -72 °C. Before being irradiated, each sample was added to a metal block surrounded in crushed dry ice and adjusted to -72 °C (approximately 5 min). Negative dark controls with and without Dye 1 were also prepared in addition to a negative light control without Dye 1. All samples were irradiated for 30 min and refrigerated thereafter at 10 °C while other samples were processed. The different forms of plasmid were then separated out via gel electrophoresis. The KI and KCl experiment was done similarly except for 10 mM and 20 mM concentrations of the salts were incorporated.

Table 2.3: For each scavenger experiment the various controls and samples were prepared as below.

| | | | | | | | | |
|------------------|---|---|---|---|---|---|---|---|
| pUC19 | + | + | + | + | + | + | + | + |
| Dye | - | + | - | + | - | + | - | + |
| Scavenger | + | + | + | + | - | - | - | - |
| Light | - | - | + | + | - | - | + | + |

?

2.2.4.5 Argon Purging Photocleavage Experiment

Since oxygen contributes to photobleaching and also plays a vital role in the photocleavage mechanisms, an argon purging assay was conducted to determine the effects oxygen might have on the photocleavage process by Dye 1. Four samples containing 10 mM phosphate buffer pH 7.0, 50 µM of Dye 1, and 38 µM bp of pUC19 were prepared in addition to two reference of 10 mM phosphate buffer and 38 µM bp of pUC19 with equal amounts of DMSO as the four samples (Table 2.6). Two samples were purged with air and two with argon for a total of 60 s and the tubes were immediately capped. After equilibrating for 5 min, one of each of the purged samples was subjected to dry ice conditions (-72 °C) or room temperature (24 °C). After adjusting to the respective temperatures, the samples were individually irradiated with the 780 nm 83 mW laser. After 30 min, the samples were left at 10 °C and then the different forms of plasmid were separated out via gel electrophoresis.

Table 2.4: The below setup for the argon purging experiment was used to determine the effects oxygen may have in the photocleavage mechanism.

| | | | | | | | |
|-------------------|----|-------|-----|---|-----|-------|-----|
| Dye | — | + | + | ? | — | + | + |
| Purging | — | Argon | Air | ? | — | Argon | Air |
| Temp. (°C) | 24 | 24 | 24 | ? | -72 | -72 | -72 |

?

2.2.4.6 Binding Mode Investigation via Photocleavage Inhibition

To further investigate particular binding modes for Dye 1, an inhibition assay based on compounds with known DNA binding modes provided information regarding the DNA interactions of Dye 1. The assay used equal concentrations of inhibitors methyl green (M), pentamidine (P), and ethidium bromide (E) with 70 μ M Dye 1 in samples containing 38 μ M bp pUC19 and 10 mM phosphate buffer pH 7.0. Three samples were pre-equilibrated with Dye 1 for 5 min and three other samples were pre-equilibrated with the inhibitors for 5 min. The samples pre-equilibrated with inhibitors were then equilibrated with Dye 1 for 5 min and vice versa. Additionally, dark controls and a reference containing 38 μ M bp pUC19, 10 mM phosphate buffer pH 7.0, and 70 μ M Dye 1 were prepared. A negative control containing 38 μ M bp pUC19, 10 mM phosphate buffer pH 7.0, and equal amounts of DMSO was also included. The prepared samples were arranged as seen in Table 2.7. The samples were irradiated using the 780 nm 83 mW laser for 30 min after adjusting the temperature of each sample to -72 °C. The different forms of plasmid were then separated out via gel electrophoresis.

Table 2.5: The inhibitors consisted of methyl green (M), ethidium bromide (E), and pentamidine (P). Dye 1 (D) was equilibrated in rows 4-6 first and equilibrated in rows 7-9 last.

| | | | | | | | | | |
|------------------|---|---|---|-----|-----|-----|-----|-----|-----|
| Dye | — | + | + | + | + | + | + | + | + |
| Inhibitor | — | — | — | D+M | D+E | D+P | M+D | E+D | P+D |
| Light | + | + | — | + | + | + | + | + | + |

?

3 RESULTS

3.1 UV/Visible Spectrophotometry

In addition to determining the appropriate wavelength to irradiate individual dyes, UV-visible spectroscopy can provide evidence of stability in particular media, whether a dye is sufficiently interacting with DNA, the type and degree of aggregation, as well as many other physical phenomena. Polar aprotic solvents, in this case DMSO, are particularly useful for dissolving and storing dyes because of their hydrophobic structures and polar delocalized charge. Therefore, it is essential to understand their stability and aggregation state at relevant concentrations. Additionally, comparing the UV-visible spectra of different dyes in DMSO can afford an expedient comparison of substituent effects on molar absorptivity and hypsochromic/bathochromic shifts in spectra. The three time courses for Dyes **1-3** can be seen in Figure 3-1 below.

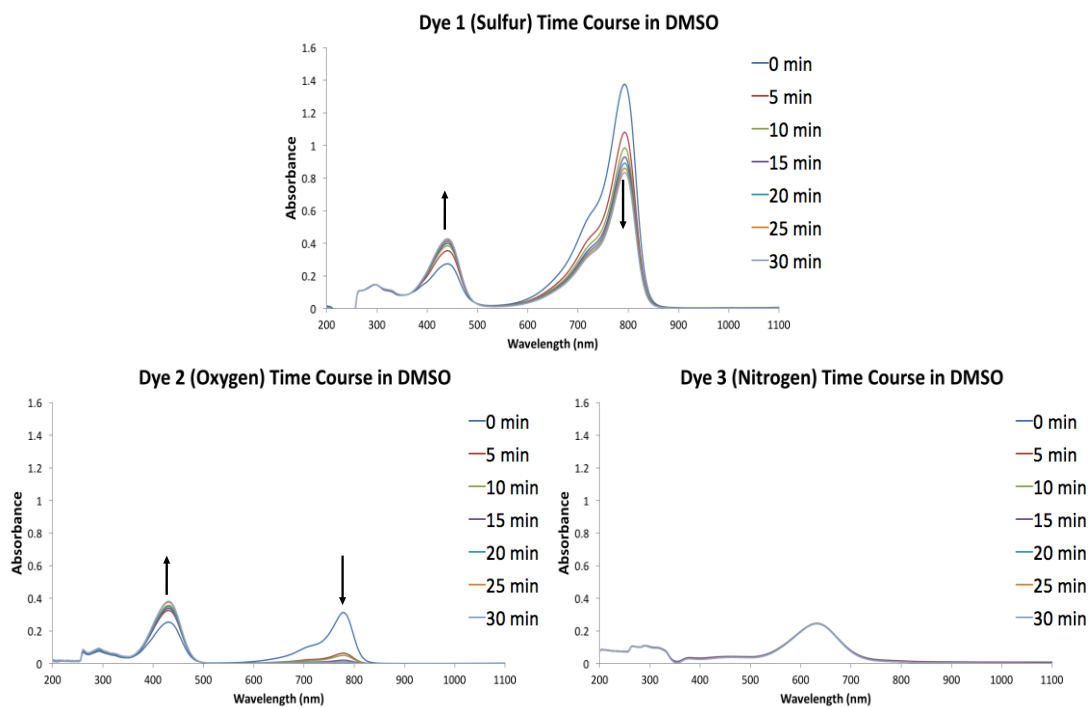


Figure 3-1: This figure shows the changes in aggregation over time in DMSO for 10 μ M of Dyes 1-3. Absorption spectra recorded in 5 min increments.

3.1.1 Absorbance Spectra in DMSO and Methanol

Figure 3-1 shows the change in absorbance and relative stability over time for 10 μM concentrations of Dyes **1-3** in DMSO. It should be noted that besides the sulfur to oxygen substitution, the structures are also different in regards to the presence of a quaternary amine on the oxygen analog. However, λ_{max} for Dye **1** (793 nm) is slightly red-shifted (15 nm shift from 788 nm) which agrees with oxygen-sulfur substitutions in other polymethine dyes.¹⁸ An unusual increase in absorption between 400 and 500 nm is seen for Dyes **1** and **2** in the visible region with Dye **2** showing a more rapid increase in absorption over time. This cannot be considered a different aggregate form since the phenomenon is occurring much farther down (blue region) the absorption spectra. Since this was only observed with Dyes **1** and **2**, absorption spectra were obtained in methanol using 5 μM concentrations to determine if this was a solvent-related effect. Figure 3-3 shows a more consistent comparison with similar oxygen and sulfur substituted heptamethine analogs showing similar absorption effects.

When comparing the initial spectra at $t = 0$ min for Dyes **1-3** in Figure 3-2, the effects of the sulfur substitution can be seen not only in bathochromicity, but also in the increase in molar absorptivity at their respective absorption peaks. A better comparison can be seen in Figure 3-3, where no change in absorption was observed over time in methanol with lambda max of Dye **1** and **2** below 1.0 AU. Both oxygen and sulfur have similar valence shells, however, sulfur has additional p and s orbitals that can contribute to an expanded valence shell while oxygen is considerably more electronegative than sulfur. The effects sulfur has on the absorption spectrum of the cyanine dye is notable given the advantage of high molar absorptivity in photosensitizers. The decrease in molar absorptivity seen in Dye **3** when compared to Dye **1** is notable. This may be attributed to the centric-localized positive charge at the meso position of the polymethine

bridge on Dye **3** that is seen with many nitrogen-substituted cyanine dyes.³⁹ This form is known as a bis-dipole and can limit the compound in terms of applications in photodynamic therapy within the therapeutic window.^{3,39}

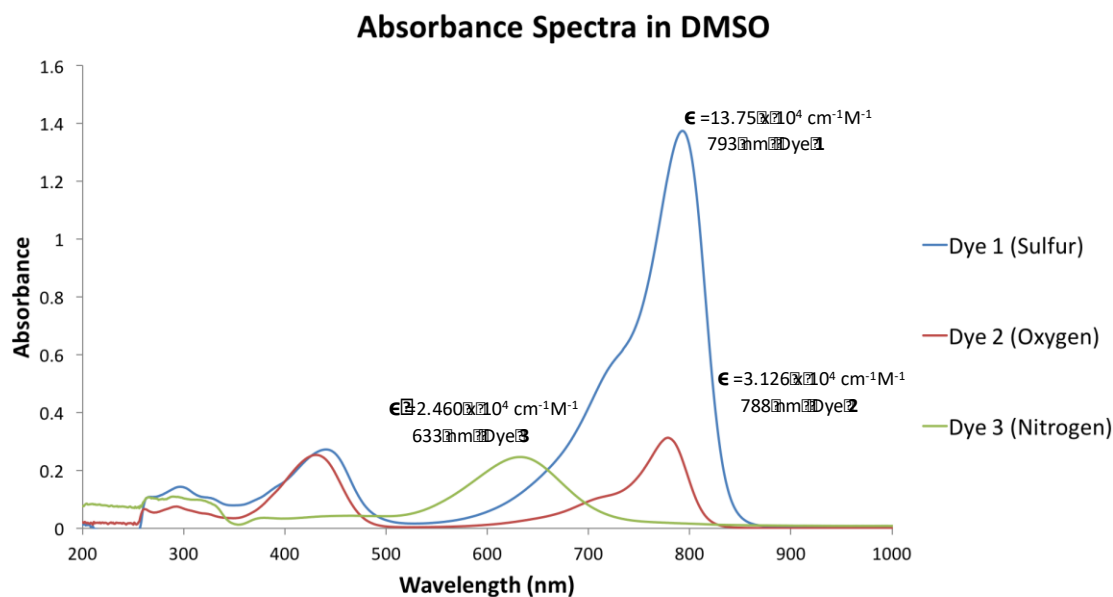


Figure 3-2: The absorption spectra of Dyes **1-3** in DMSO at $t = 0$ min (all dye concentrations were $10 \mu\text{M}$). All molar extinction coefficients are rough estimates based on the above trials only.

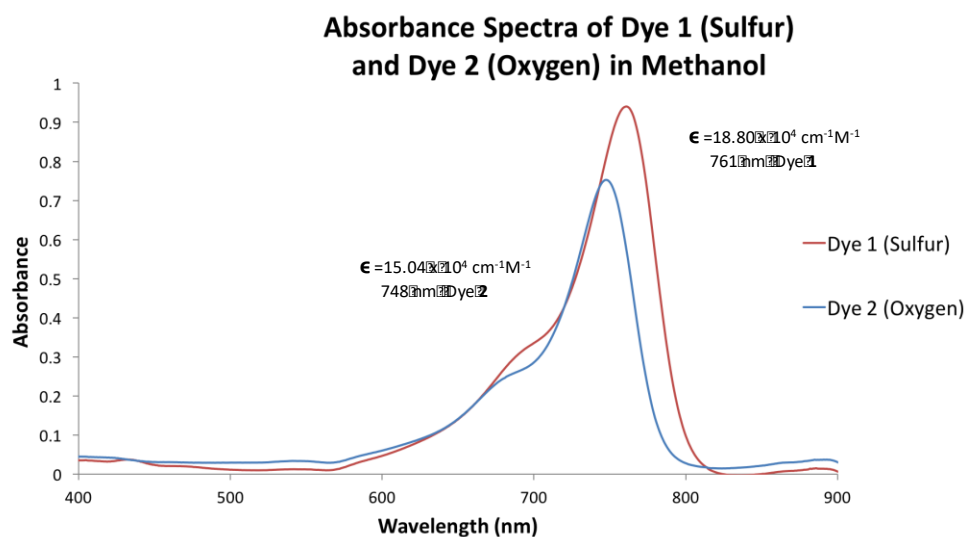


Figure 3-3: The absorption spectra of Dyes **1** and **2** in methanol at $t = 0$ min (both dye concentrations were $5 \mu\text{M}$). Both molar extinction coefficients are rough estimates based on the above trials only.

3.1.2 Absorbance Spectra with CT-DNA

Since Dye **1** showed strong absorption in DMSO and methanol at a λ_{max} value near the 780 nm output of GaAlAs diode lasers, the absorption spectra of Dye **1** in the presence and absence of CT-DNA in a 10 mM phosphate buffer pH 7.0 were obtained before continuing with photocleavage experiments (Figure 3-3). Although there is some degradation of the dye in the absence of DNA (Figure 3-3B), the increased stability of the Dye **1** in the presence of DNA is apparent over the 30 min time course (Figure 3-3C). The spectra indicate the evident interaction and induced stability the dye has in the presence of DNA with little decrease on the absorption and an observed slight red-shift upon DNA addition. This is typical of DNA-dye complex absorption spectra, providing further evidence that Dye **1** is sufficiently interacting with DNA.

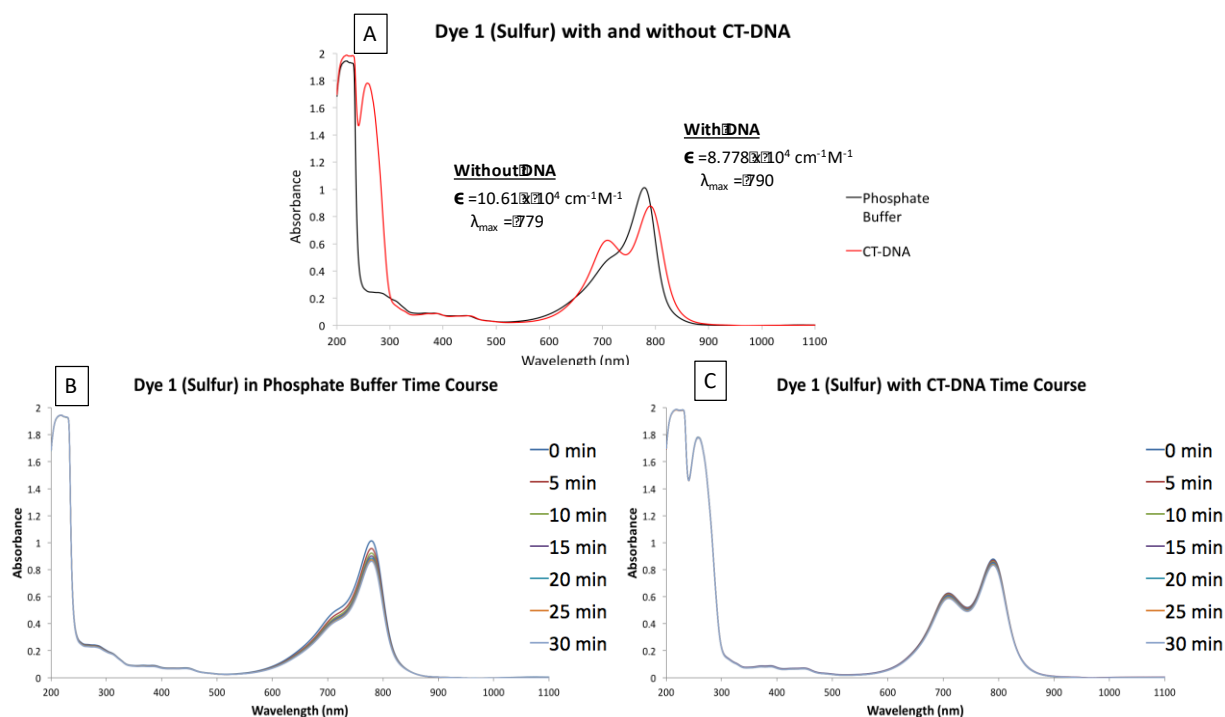


Figure 3-4: The absorbance spectra of 10 μM Dye **1** in the presence and absence of CT-DNA (150 μM bp). There is a slight red-shift and hypochromicity in the Dye-DNA complex spectrum when compared to the dye absorption spectrum in 10 mM phosphate buffer pH 7.0.

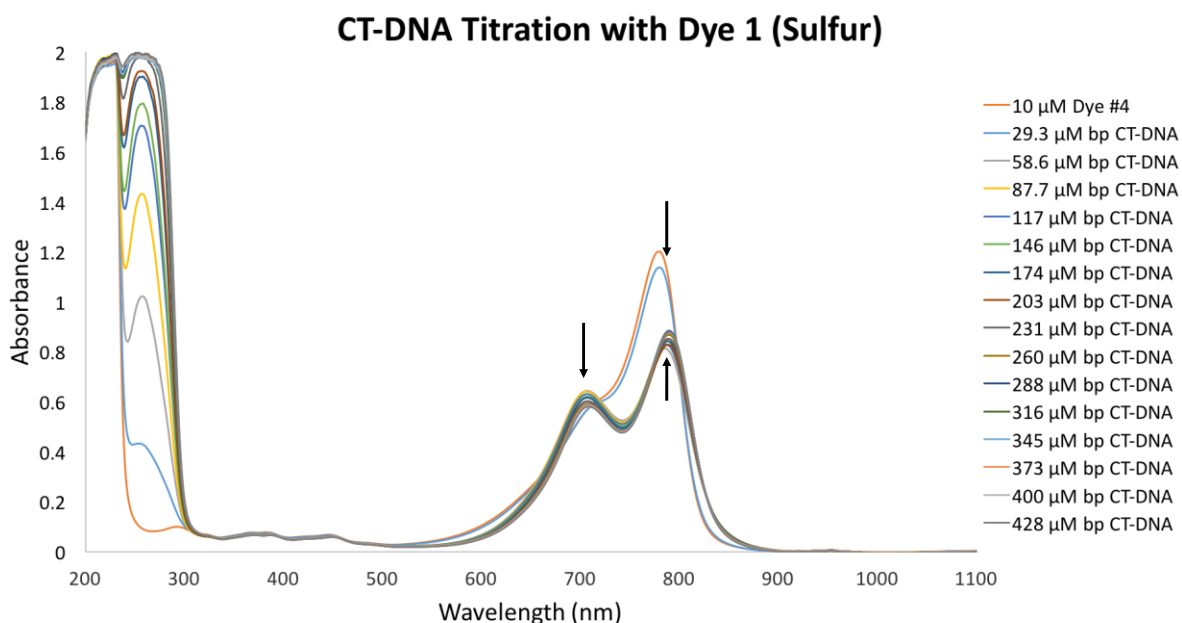
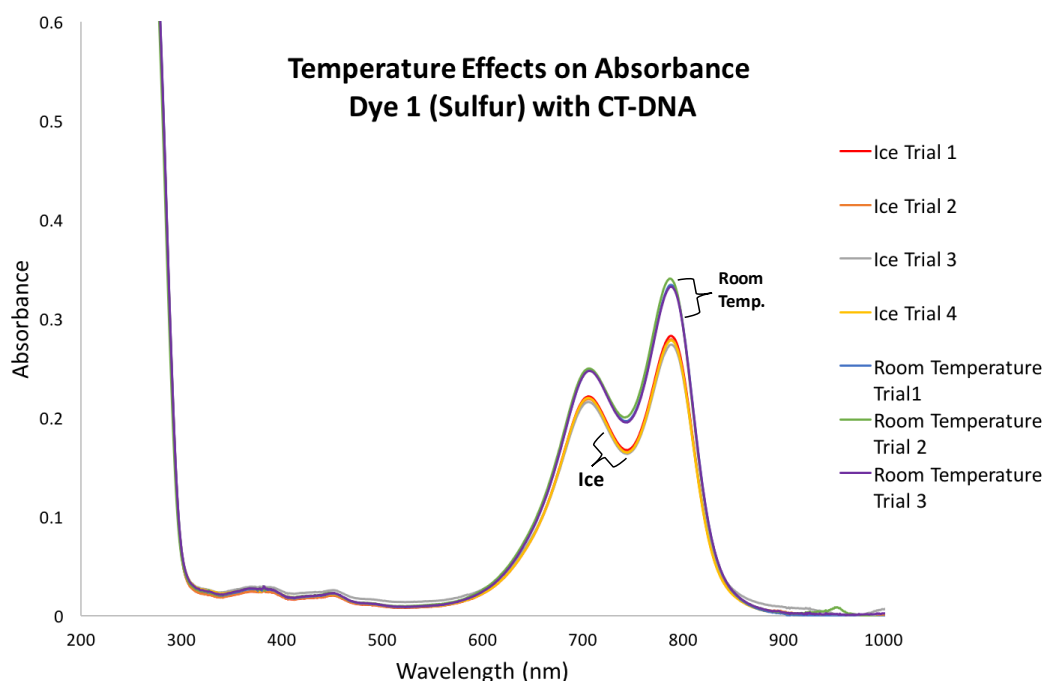


Figure 3-5: The CT-DNA titration with Dye 1 in a 10 mM phosphate buffer pH 7.0 shows a sharp absorption decrease at slightly below 60 μM bp CT-DNA. All concentrations of CT-DNA were corrected for sample dilutions.

In order to determine the concentration of DNA needed to completely bind Dye 1 and optimize the experimental parameters for binding mode studies via CD spectroscopy, a CT-DNA titration was performed using a 10 μM concentration of Dye 1. As seen in Figure 3-4, there is an almost immediate drop in absorbance after the second addition of CT-DNA with a corrected concentration of 58.6 μM bp. After each subsequent addition of CT-DNA, slight changes in the DNA-dye complex absorption spectra occur with the absorption peak at 710 nm decreasing and the peak at 792 nm increasing in intensity. The titration was continued until there was no observable difference in three consecutive absorbance spectra. The concentrations of CT-DNA that provided the highest absorbance at 710 nm (100 μM bp and 120 μM bp) were then used in CD/ICD experiments for the two dye concentrations (10 μM and 20 μM) due to the reduced sensitivity of the CD detector above 750 nm.

3.1.3 Temperature Effects on Aggregation and Absorbance

In order to determine whether or not differences in aggregation or increased absorbance are possibly contributing changes in photocleavage when lowering temperatures, it was necessary to record absorption spectra of Dye **1** after subjecting the DNA-dye complex to the different temperature conditions. The results in Figure 3-6 show changes in absorption spectra with a modest absorption decrease at low temperatures. Interestingly, no precipitation was observed within the cuvette for any of the samples. The results suggest that any potential changes in absorbance as temperatures decrease may influence to some extent the photocleavage observed. However, this does not account for the increase in photocleavage yields at lower temperatures.



*Figure 3-6: Temperature effects on absorbance and aggregation were determined to see if any difference could explain possible increases in photocleavage yields at low temperatures. Dye **1** (5 μM) in the presence of 60 μM bp CT-DNA and 10 mM phosphate buffer pH 7.0 subjected to 2 $^{\circ}\text{C}$ and 24 $^{\circ}\text{C}$ for 10 min before spectra were immediately obtained. A total of four trials were done at 2 $^{\circ}\text{C}$ and three at 24 $^{\circ}\text{C}$ with consistent results between each trial. An obvious decrease in the DNA-dye complex absorption spectra is visible at 2 $^{\circ}\text{C}$.*

3.1.4 Photobleaching at Decreasing Temperature

To determine if decreased dye photobleaching was occurring at lower temperatures, a simple UV-Visible spectrophotometric assay was performed. The results indicate that photobleaching is dramatically reduced at colder temperatures as seen in Figure 3-7. Within 3 min of irradiation at 780 nm, the samples at room temperature were almost completely photobleached, signifying the instability of the sulfur-incorporated dye. Peceli et al. also indicated that although sulfur dyes maintain significantly higher triplet quantum yields through enhanced intersystem crossing, the PDs are also quite unstable when irradiated. This provides strong evidence that colder temperatures are directly affecting the apparent photocleavage by Dye 1 in the presence of DNA through decreased photobleaching.

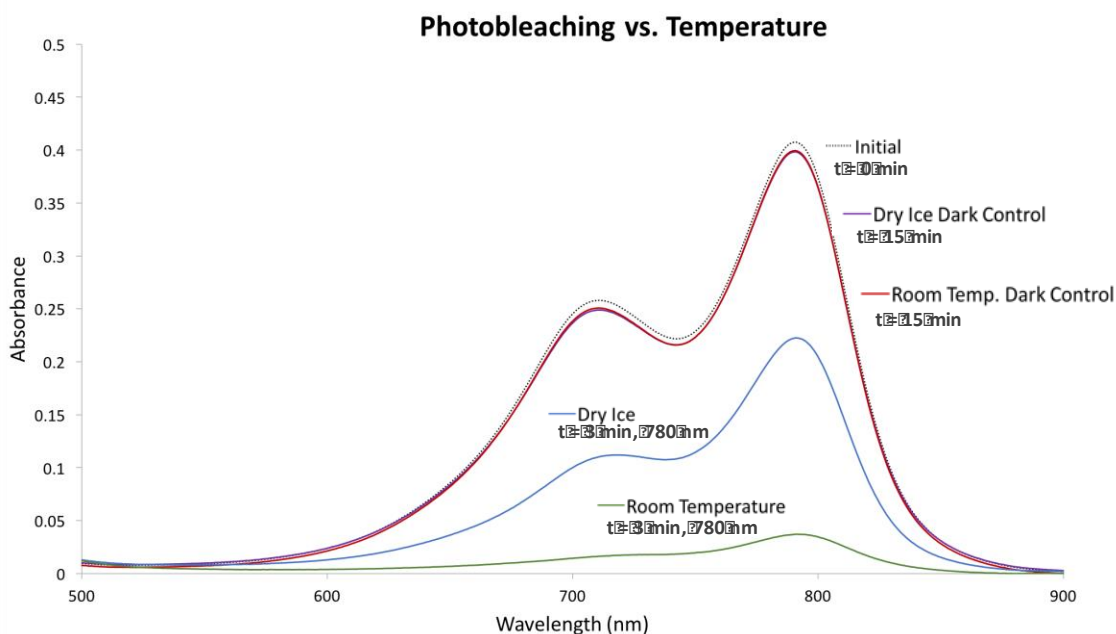
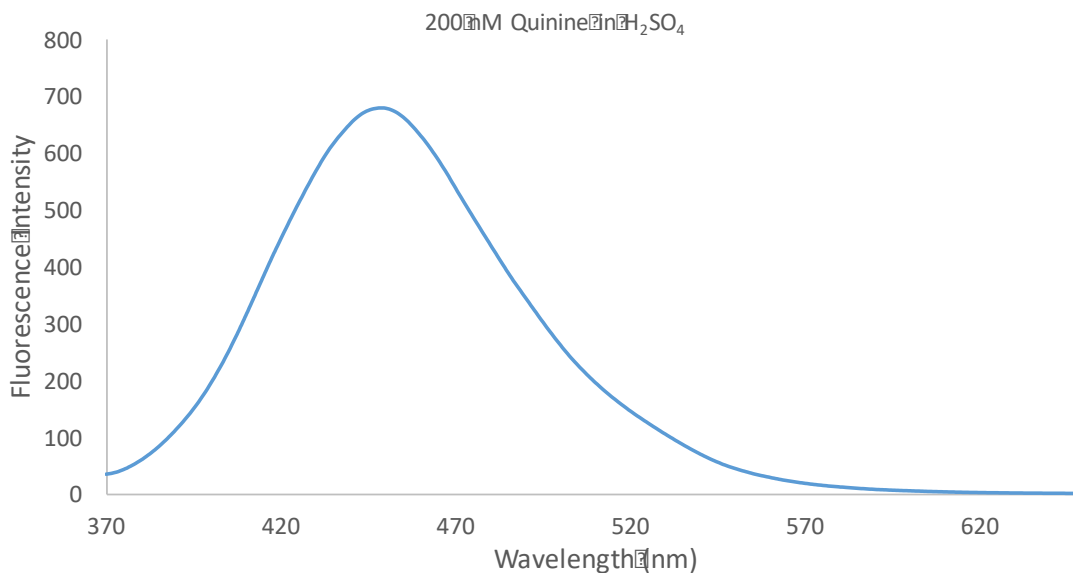


Figure 3-7: The absorption spectra before and after irradiation (780 nm with 83 mW for 3 min) at room temperature and dry ice conditions which show the degree of photobleaching under the different temperatures. All samples contained 60 μ M bp CT-DNA, 10 mM phosphate buffer pH 7.0, and 5 μ M of Dye 1. Spectra for dark controls were obtained after the spectra of the irradiated samples were obtained. The initial spectrum was used as a reference for any degradation that may have taken place over the course of the entire experiment.

3.2 Fluorescence Spectroscopy

As discussed in the paper presented by Peceli et al., sulfur-incorporated PDs tend to have very rapid intersystem crossing rates and therefore exhibit relatively negligible fluorescent quantum yields.¹⁸ In order to gain insight on intersystem crossing rates of Dye **1**, it was essential to determine its propensity for fluorescence. As seen in Figure 3-9A below, Dye **1** in DMSO exhibited low levels of fluorescence when compared to a quinine reference of the same concentration (Figure 3-8). When small increments of CT-DNA were added to Dye **1** in the presence of 10 mM phosphate buffer and 10 mM EDTA, the compound showed no fluorescence (Figure 3-9B). This suggests that nonradiative intersystem crossing (or internal/external conversion) are the possible pathways for singlet excited state deactivation. Absorbance spectra were obtained using a spectrophotometer and are shown as reference in Figure 3-9.



*Figure 3-8: The fluorescence emission spectrum of 200 nM quinine in 500 mM sulfuric acid used as reference for Dye **1** fluorescence in the presence and absence of CT-DNA.*

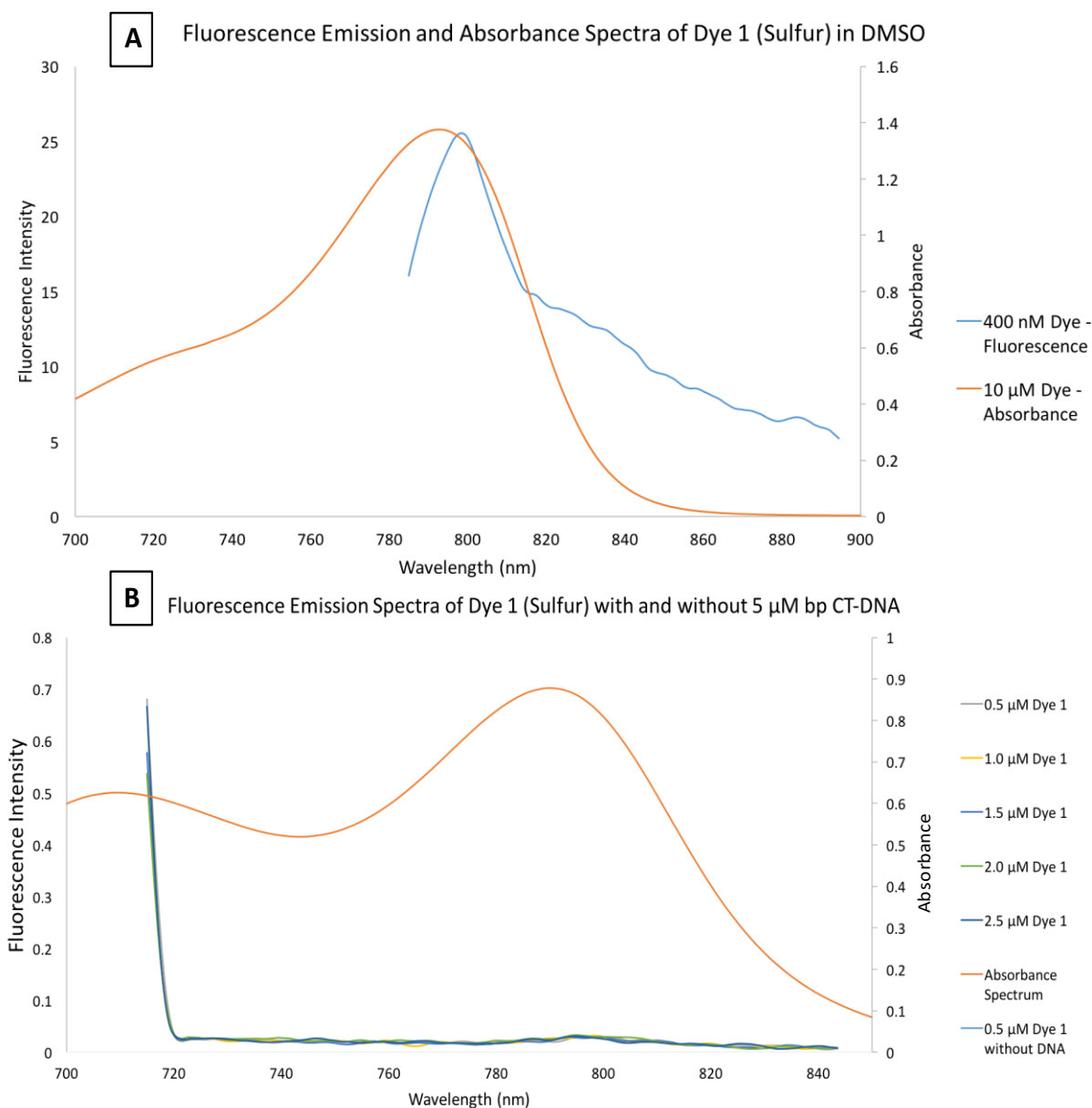


Figure 3-9: The above emission spectra were obtained using a fluorimeter and the absorbance spectra were obtained using a separate spectrophotometer. (A) Low fluorescence is observed for 400 nM Dye 1 in DMSO when compared to 200 nM quinine reference in Figure 3-8. The absorbance spectrum shown as a reference consisted of 10 μM Dye 1 in DMSO. (B) Fluorescence of 400 nM Dye 1 in the presence and absence of 5 μM bp CT-DNA in 10 mM phosphate buffer pH 7.0 and 10 mM EDTA indicates no cyanine fluorescence is observed when in the presence or absence of DNA in a phosphate buffer solution. EDTA was used to chelate any trace metals that would otherwise diminish any potential fluorescence by Dye 1. The absorption spectrum shown as reference consisted of 10 μM Dye 1 with 150 μM bp CT-DNA in 10 mM phosphate buffer pH 7.0.

3.3 CD Spectroscopy

Based on the CT-DNA titration using 20 μM of Dye **1** (Figure 3-5), it was determined that 60 μM bp to 100 μM bp of CT-DNA would serve as the optimal concentration range for showing the strongest induced CD signal to interpret DNA binding mode in the near-infrared range. Given the limits of the CD detector at longer wavelengths (as seen in the evident noise above 750 nm in Figure 3-10) these concentrations provided the strongest absorption of the DNA-dye complex at the 710 nm absorption maximum. A concentration of 100 μM bp of CT-DNA gave the strongest induced CD signal from 700 to 710 nm in Figure 3-10. As seen in the accompanying absorbance spectrum, this correlates with the peak at 710 nm of the DNA-dye complex indicating interaction between Dye **1** and CT-DNA.

As mentioned by Garbett et al. about binding mode determination and ligand affinity through CD spectroscopy, intercalators display small induced CD signals at absorption maxima when compared to groove binders (contingent on the oscillator strength of the ligand). However, signal strength varies according to the probable number of orientations of the ligand within a groove, therefore, major groove binders or intercalators that partially fit between base pairs show a variety of signals.³⁸ In Figure 3-10, a weak, negative induced CD signal for Dye **1** can be seen suggesting that either intercalation or monomeric groove binding is occurring. However, based on the structure of Dye **1**, it seems less likely that any intercalation is occurring due to the indolium ring system. A more robust aromatic system that integrates more than two rings on either side of the polymethine bridge would engage in more van der Waals interactions within the base base pairs of DNA similar to polycyclic aromatic hydrocarbons.⁸ Moreover, the indolium ring system incorporated into Dye **1** has two methyl groups which purposely inhibit intercalation through steric hindrances. Therefore, the compound should not be capable of proceeding through

this binding mode. In light of this, the CD spectroscopic results point to groove binding interactions.

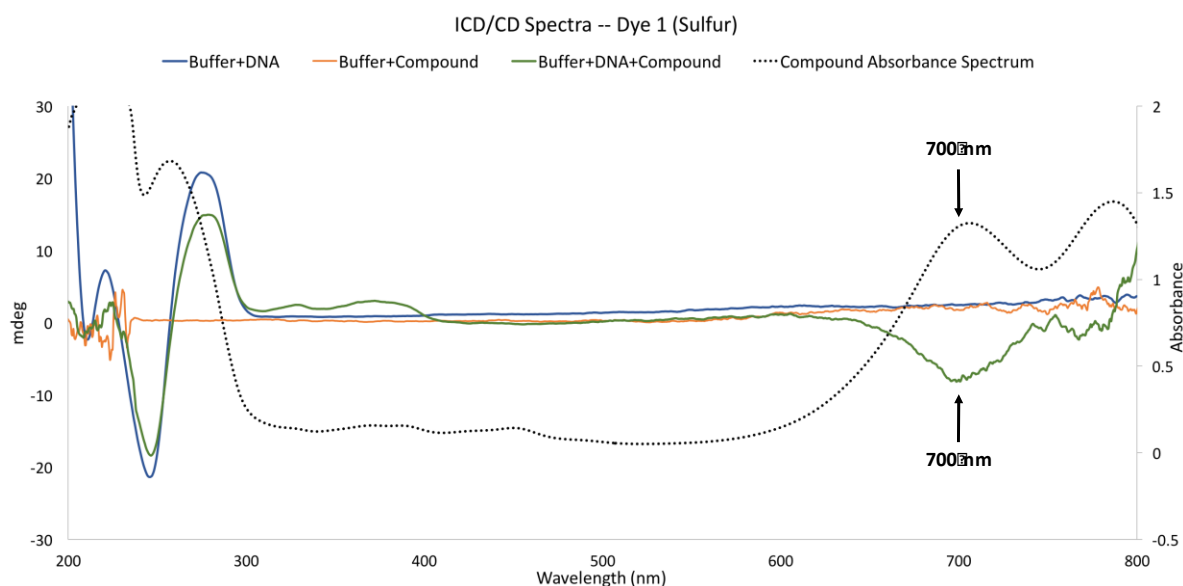


Figure 3-10: The CD and induced CD spectra of 20 μ M Dye 1 in the presence of 10 mM phosphate buffer pH 7.0 and 100 μ M bp CT-DNA. The absorbance spectrum sample contained 20 μ M Dye 1, 10 mM phosphate buffer pH 7.0, and 100 μ M bp CT-DNA as well.

3.4 Photocleavage Experiments

3.4.1 Decreasing Temperature Effects

Due to the possibility of thermally-induced DNA cleavage arising from heat from the lasers, most photocleavage experiments were done on ice. When dry ice was additionally employed in the original photocleavage experiments of Dye 1, the low temperature produced an unexpected and remarkable enhancement in photocleavage yields as seen in Figure 3-11 (See appendix for other three trials in Figures 0.1-0.3). Therefore, low-temperature effects were investigated in this thesis to determine or pinpoint the specific cause of these results. Interestingly, in Figure 3-12 a strong correlation between temperature and % nicked plasmid at 24 $^{\circ}$ C, 0 $^{\circ}$ C, and -72 $^{\circ}$ C was observed, indicating physical state (solid vs. liquid) could not account for the increase cleavage.

It should be noted that the increase in cleavage was observed both in the lower temperature liquid (0 °C) and solid states (-72 °C). Dark controls were also included in a separate experiment and can be seen in the Appendix (Figure 0.4).

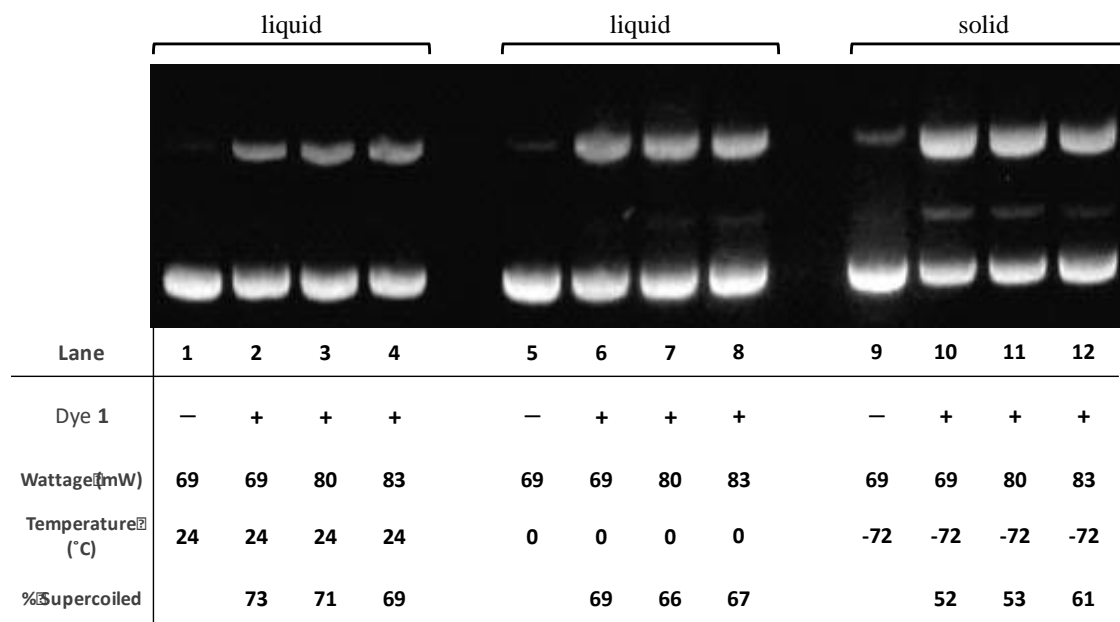


Figure 3-11: As the temperature conditions are decreased an obvious increase in nicked and linear forms of plasmid DNA can be observed, indicating either an indirect or direct correlation between temperature and photocleavage exists. Samples contained 38 μ M bp pUC 19, 10 mM phosphate buffer pH 7.0, and 50 μ M of Dye 1 or equal amounts of DMSO (Lanes 1, 5 and 9).

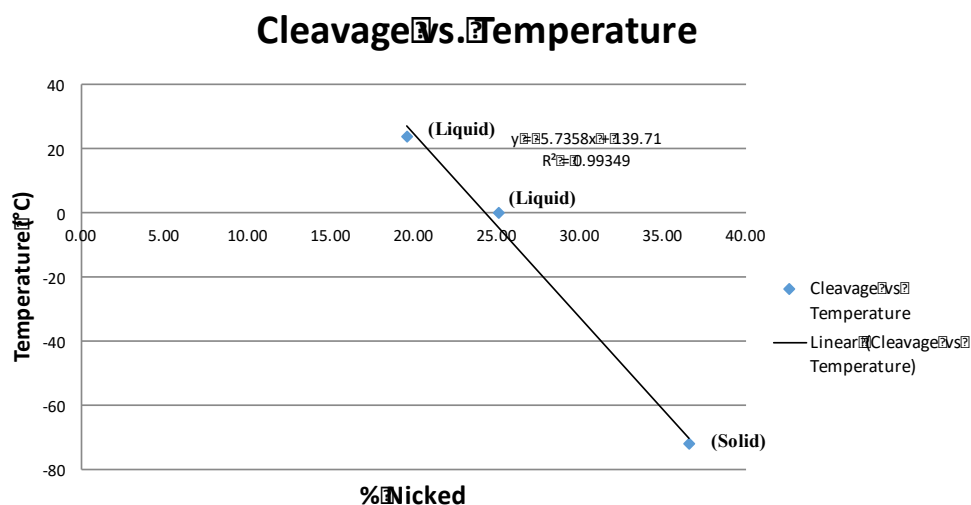
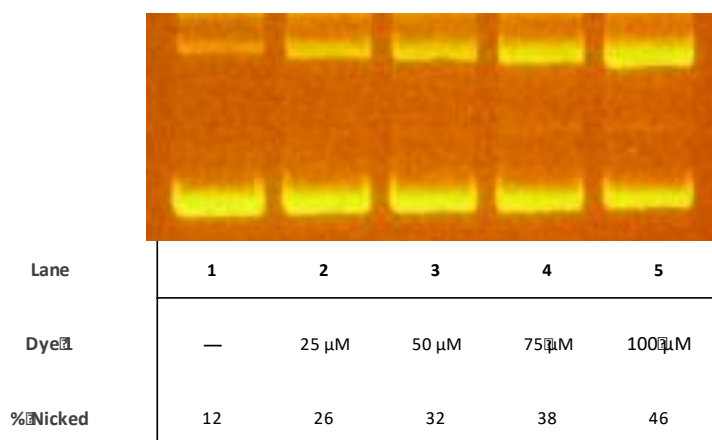


Figure 3-12: This graph shows a correlation between the three temperatures used in the photocleavage experiments with yields of nicked plasmid. These temperatures were chosen based on the different available cooling methods that provided consistent results.

3.4.2 Photocleavage Titration

The photocleavage titration experiment was done in order to optimize concentrations of Dye **1** for the different samples of plasmid that were prepared throughout the course of research. The titration seen in Figure 3-13 shows the typical correlation seen between pUC19 photocleavage and the concentration of Dye **1**. The difference in % nicked is more prominent between 25 μM and 50 μM of dye and continues to increase between 50 μM and 100 μM . Most experiments were carried out at 50 μM of Dye **1** except for the preliminary kinetics experiment, argon purging, and the photocleavage inhibition assay which were carried out at 70 μM . This is because this yielded similar photocleavage yields between the various pUC19 stocks that were prepared. It should be noted that the linear form of the plasmid appears at concentrations higher than 50 μM despite the lack of diffusion of molecules at $-72\text{ }^{\circ}\text{C}$.



*Figure 3-13: This photocleavage titration was done to show the increase in photocleavage as a function of dye concentration. Samples contained different concentrations of Dye **1** (Lanes 2-5) with 10 mM phosphate buffer pH 7.0 and 38 μM bp pUC19 with a reference containing equal amounts of DMSO (Lane 1). Samples were irradiated at 780 nm with 83 mW laser for 30 min at $-72\text{ }^{\circ}\text{C}$.*

A preliminary kinetics experiment using 50 μM and 70 μM concentrations of Dye **1** at 30 min and 60 min indicate little to no difference between the two allotted irradiation times (Figure

3-14). Based on this information, the first successful kinetics experiment was performed using 70 μM Dye 1 giving the % supercoiled observed in previous irradiation experiments. The differences in % supercoiled for the kinetics experiment seen in Figure 3-15 suggest that either the assay needs to be adjusted or multiple trials must be completed to obtain consistent data. Fu

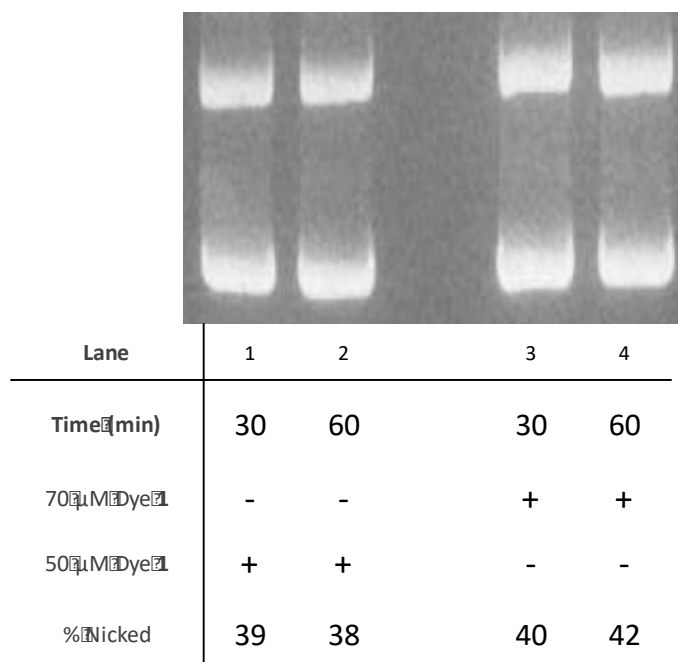



Figure 3-14: The initial photocleavage kinetics experiment to determine the sufficient end time for future kinetics experiments. Samples contained either 50 μM or 70 μM concentrations of Dye 1 in the presence of 10 mM phosphate buffer 7.0 and 38 μM bp pUC19. Samples were irradiated using the 83 mW 780 nm laser for 30 or 60 min at -72 $^{\circ}\text{C}$.



| Lane | 1 | 2 | 3 | 4 | 5 | 6 | 7 | 8 | 9 | 10 | 11 | 12 | 13 |
|---------------|----|----|----|----|----|----|----|----|----|----|----|----|----|
| Time (min) | 1 | 2 | 3 | 4 | 6 | 8 | 10 | 15 | 20 | 30 | 30 | – | – |
| Dye | + | + | + | + | + | + | + | + | + | + | – | + | – |
| 780nm (83mW) | + | + | + | + | + | + | + | + | + | + | + | – | – |
| % Supercoiled | 84 | 75 | 71 | 66 | 66 | 61 | 58 | 56 | 56 | 50 | 94 | 94 | 94 |

Figure 3-15: The kinetics photocleavage assay to determine the rate order of the photocleavage reaction. Samples contained 70 μM of Dye 1, 10 mM phosphate buffer pH 7.0, and 38 μM bp pUC19. Samples were irradiated with a 780 nm 83 mW laser at $-72\text{ }^\circ\text{C}$ for the times listed above.

Inconsistencies in the % supercoiled after irradiation can be seen in the kinetic graphs in Figure 3-16, Figure 3-17, and Figure 3-18, which test for second, first, or zero order rate laws. Even when taking out outliers, the R^2 values are too low to make definitive conclusions on reaction order. Further optimizing of this particular kinetics assay is necessary for more consistent results. The solid matrix employed may affect the reaction rate and rate law in a different manner than reactions carried out at higher temperatures. Since photocleavage yields were shown to be heavily affected by temperature this complicates designing an adequate experimental setup that would provide consistent results for determining the rate order.

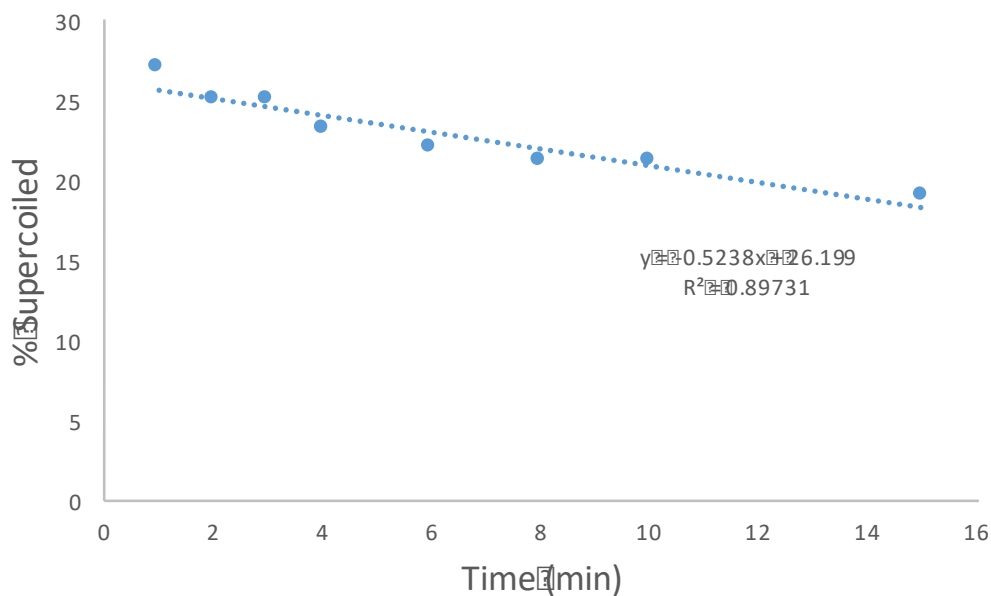


Figure 3-16: This graph shows the % supercoiled vs. time as a test for zero order reaction kinetics. The reactions were carried out consistently at $-72\text{ }^{\circ}\text{C}$. A 780 nm 83 mW laser was utilized for each sample. Two outliers (1 and 10 min) were removed and are not shown in the above plot.

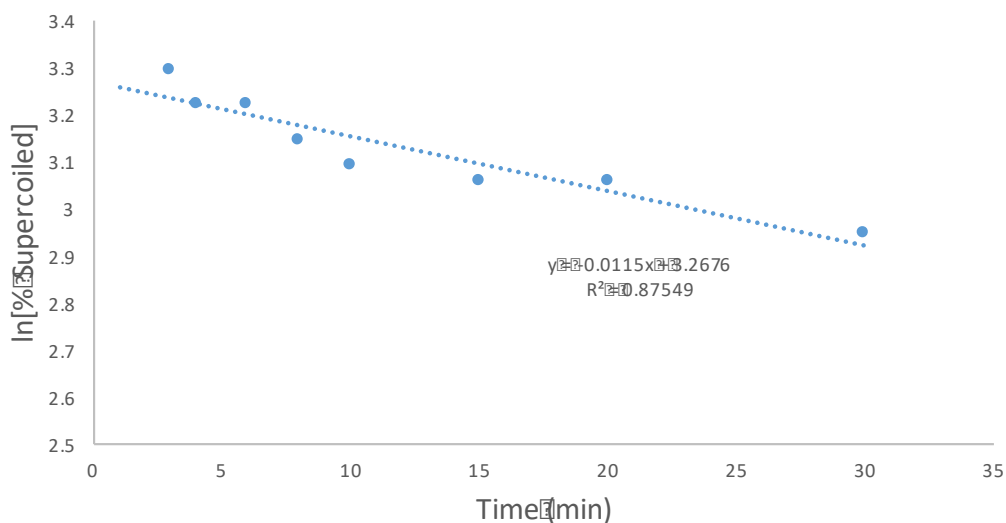


Figure 3-17: This graph shows the natural log of supercoiled concentration vs. time as a test for first order reaction kinetics. The reactions were carried out consistently at $-72\text{ }^{\circ}\text{C}$. A 780 nm 83 mW laser was utilized for each sample. Two outliers (1 and 10 min) were removed and are not shown in the above plot.

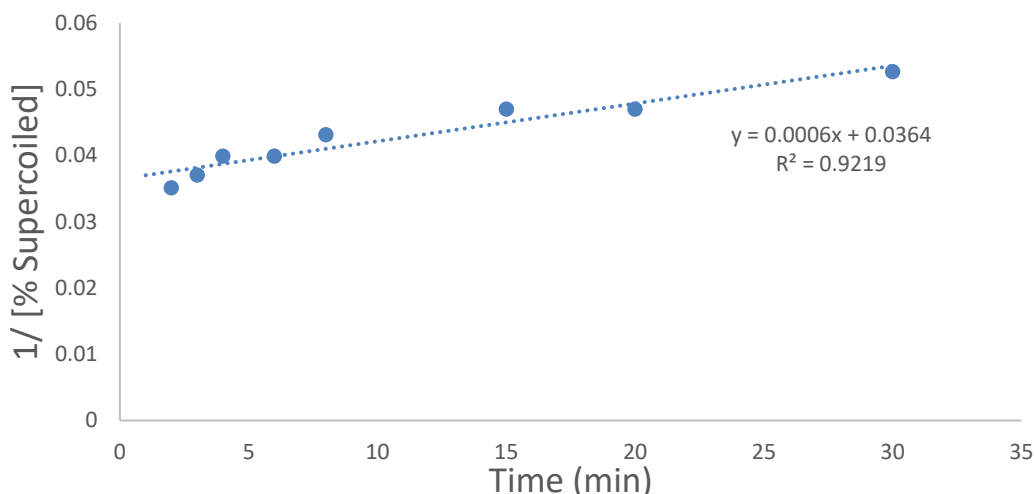


Figure 3-18: This graph shows the reciprocal plot of supercoiled concentration vs. time which tests for second order reaction kinetics. The reactions were carried out consistently at -72 °C. A 780 nm 83 mW laser was utilized for each sample. Two outliers (1 and 10 min) have been removed to compare the most consistent cleavage yields.

3.4.3 Scavenger Experiments and Argon Purging

The scavenger experiments and argon purging provide evidence for the involvement of specific ROS and the requisite of oxygen in the photocleavage mechanism, respectively. Sodium benzoate and potassium iodide are known to react with hydroxyl radicals ($\cdot\text{OH}$) therefore any involvement of $\cdot\text{OH}$ within the overall photocleavage mechanism can be determined based the decrease in photocleavage yields. Likewise, sodium azide is known to react with singlet oxygen ($^1\text{O}_2$) and inversely D_2O can increase the lifetime of $^1\text{O}_2$. This provides evidence for whether or not a Type II energy transfer is occurring or if the Type I electron transfer is the foremost pathway for generating ROS. Additionally, EDTA is a well-known metal chelator which can scavenge trace redox-active metals that may contribute to ROS production via Fenton-like chemistry.

By purging with argon gas, this decreases the amount of oxygen within the sample. Although oxygen is generally considered a necessary component in photocleavage mechanisms, enhanced photocleavage in anaerobic conditions can imply an oxygen-independent photocleavage

mechanism may be occurring. Additionally, ROS have been shown to cause photobleaching, therefore, reduced photobleaching may also contribute to an observed enhancement in photocleavage yields if an oxygen-independent mechanism exists.

Based on the data shown in Figure 3-19, the average photocleavage inhibition indicates an aerobic-involved photocleavage mechanism in addition to the participation of trace concentrations of redox metals found in the solution.⁴⁰ All the gels that were used to calculate % inhibition in the scavenger experiments can be seen in the Appendix (Figures 0.5-0.10).

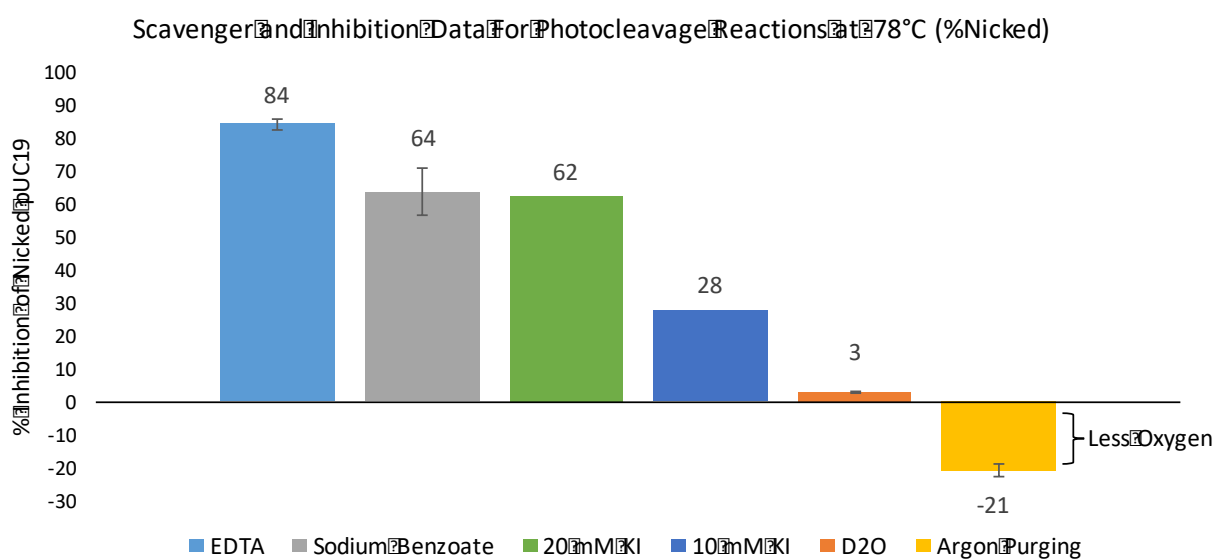


Figure 3-19: This chart consists of the averages over three trials and standard deviations of the ROS scavenger experiments (except for KI which was done in one trial) in addition to the argon purging experiments. The argon purging enhancement was calculated by the difference of % total nicked DNA between the samples purged with air and the samples purged with argon divided by the samples purged with air. Similar calculations were done for the other scavenger experiments with the difference of % total nicked DNA without scavenger and the % total nicked DNA with scavenger divided by % total nicked DNA without scavenger.

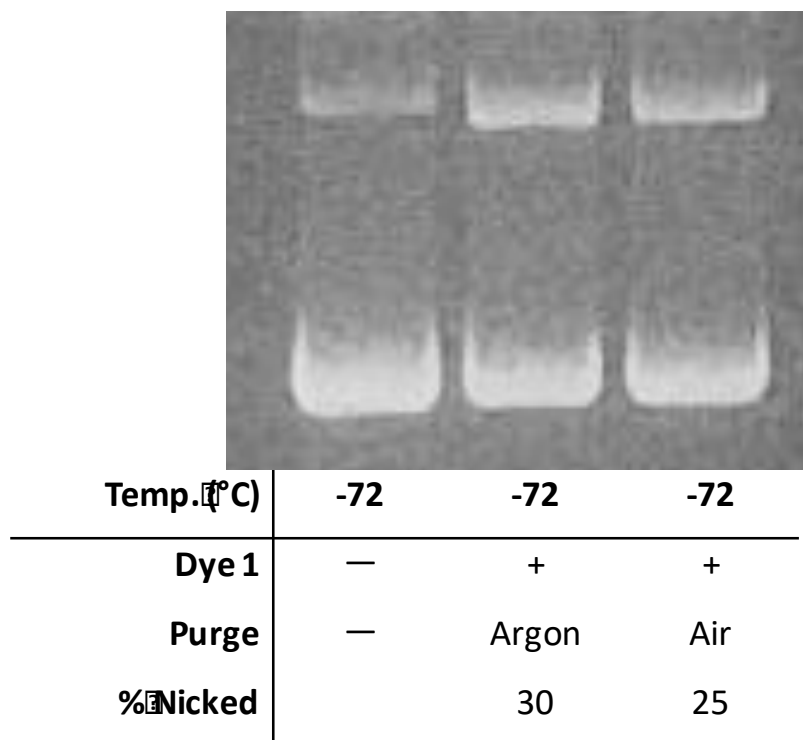


Figure 3-20: The photocleavage experiment using air and argon purging to determine the role molecular oxygen plays in the photocleavage mechanism. Samples were gently purged with argon or air for 1 min. Samples containing 70 μM Dye 1 or equal amounts of DMSO (Lane 1), 10 mM phosphate buffer pH 7.0, and 38 μM bp pUC19 were irradiated using 780 nm 83 mW lasers for 30 min after adjusting to the appropriate temperature.

Figure 3-20 shows the notable enhancement in photocleavage when samples purged with argon and compared to samples purged with air. The above photocleavage experiment shows a increased in % nicked form DNA by 5% which represents a 20% increase when compared to the sample purged with air. This experiment was repeated four times with similar results in three of the four trials (see Appendix Figures 0.9-0.10). Hypothetically this has great implications for cancer therapeutics in addition to photosensitizing agents given their reduced efficacy in tumors with low levels of oxygen. A sulfur-involved radical mechanism has been proposed and discussed previously in literature, however, extensive studies have yet to be performed.²⁴

3.4.4 Binding Mode Investigation via Photocleavage Inhibition

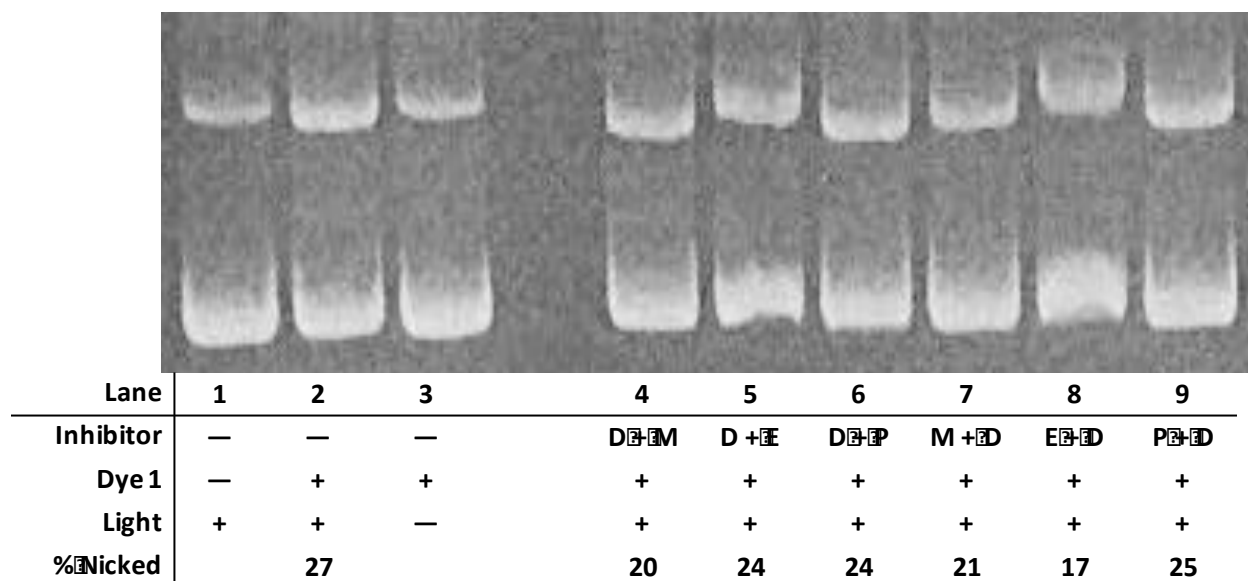
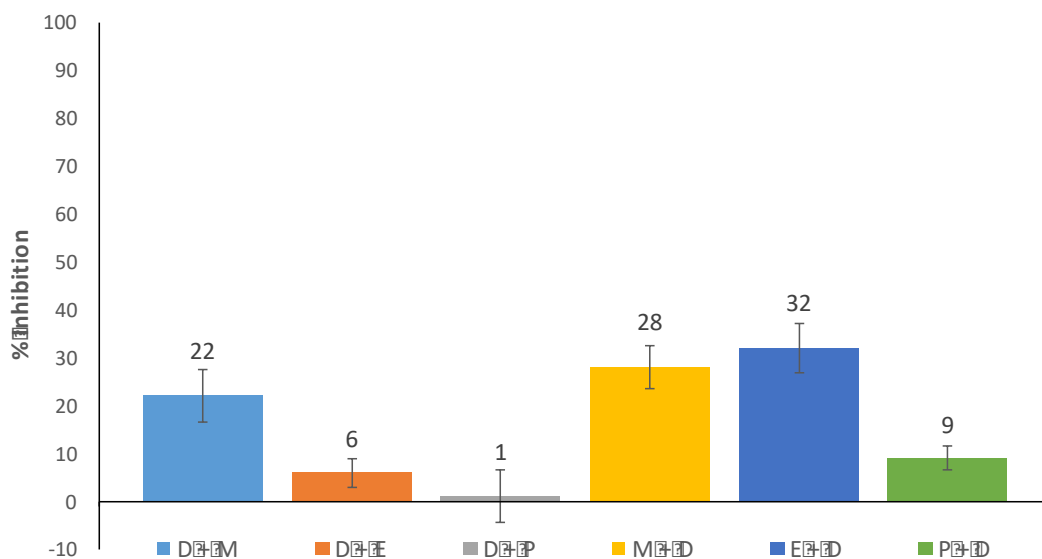


Figure 3-21: The photocleavage inhibition binding investigation consisted of using compounds with established DNA binding modes to inhibit photocleavage by Dye 1. The samples contained equal concentrations (70 μ M) of either methyl green (M), ethidium bromide (E), or pentamidine (P) with 70 μ M of Dye 1. The samples also contained 10 mM phosphate buffer pH 7.0 and 38 μ M bp pUC19. The samples were equilibrated for 5 min with Dye 1 first for 5 min (D + I) or with the inhibitor first for 5 min (I + D) and then vice versa. Samples were kept at -72 °C while each were individually irradiated using an 83 mW 780 nm laser for 30 min. The other trials can be seen in the Appendix Figures 0.11-0.12)

The binding mode investigation through photocleavage inhibition was used to accommodate the UV-visible absorption and CD spectroscopy data. By using reagents with established binding modes, inhibition of photocleavage in solutions equilibrated with the reagents and Dye 1 provides insight into the interactions of Dye 1 with DNA. Since these reagents do not absorb light in the presence and absence of DNA at 780 nm, the observed photocleavage can be only attributed to the absorbance of light by the DNA-dye complex (See Appendix Figure 0.13 for absorbance spectra). Most reagents showed inhibition of photocleavage by Dye 1 in every trial, especially when the reagents were equilibrated with pUC19 before adding Dye 1 (Figure 3-21). Although the most consistent inhibition was observed with methyl green (major groove binder),

the small relative amount of inhibition with the three reagents suggests that Dye **1** may have more than one binding mode.⁴¹



*Figure 3-22: This graph shows the percent inhibition of nicked DNA by compounds with known binding modes. These values represent averages over three trials with standard deviations shown through error bars. Order of equilibration of added compounds shown as either D + I or I + D. Abbreviations: Dye **1** (D), Inhibitor (I), methyl green (M), ethidium bromide (E), and pentamidine (P).*

Pentamidine is a known minor groove binder with a dissociation constant of 6.07×10^{-5} M. Little to no inhibition is observed with DNA pre-equilibrated with Dye **1** and relatively little inhibition is observed with DNA pre-equilibrated with pentamidine first (Figure 3-22). This suggests that the binding modes of Dye **1** do not likely include minor groove. Ethidium bromide is a well-known intercalator (dissociation constant of 1.00×10^{-7} M) and showed the most drastic difference in inhibition between the samples pre-equilibrated with Dye **1** and samples pre-equilibrated with ethidium bromide.⁴²⁻⁴³ However, based on the structure of Dye **1** it is unlikely that the inhibition shown in Figure 3-22 is due to competitive binding between Dye **1** and ethidium bromide. Based on the binding studies in this thesis, it is likely that Dye **1** is binding

through different orientations within the major groove and possibly through electrostatic interactions with the negatively charged phosphate backbone of DNA. Groove binding is also supported through the induced CD spectrum shown in Figure 3-10.

4 CONCLUSIONS

The effects of substituting atoms within Group 6 of the periodic table (sulfur to oxygen) is dramatic as seen in the absorption spectra. The high molar absorptivity of the sulfur compound (Dye **1**) and absence of a positively charged quaternary amine on the meso-substituted allowed for further photocleavage investigations. Furthermore, as discussed in full detail by Pascal et al. through density functional theory calculated BLA and ^{13}C NMR chemical shifts, by substituting nitrogen (Dye **3**) this creates a bis-dipole cyanine form with the positive charge being more localized at the meso position of the bridge.³⁹ This effectively shifts the absorption spectrum into the blue range and lowers the molar absorptivity of the dye and DNA-dye complex. The effect of low temperatures were shown to have little to no effect on the DNA-dye absorption spectra, indicating that changes in aggregation did not occur and could not account for the increase in photocleavage yields.

Fluorescence and internal conversion are considered competitive pathways to the nonradiative intersystem crossing pathway. Therefore, fluorescence emission spectra in the absence and presence of DNA were obtained. Minimal fluorescence in DMSO and no observed fluorescence with increasing amounts of DNA indicated that Dye **1** is a poor fluorophore. Based on the unique absorption spectrum and the lack of fluorescence, Dye **1** should be a relatively efficient photosensitizer. This is also supported by nonlinear and linear optical properties of sulfur-incorporated squaraine dyes investigated by Peceli et al. through femto- and picosecond

pulsed lasers via single and double-pump probes and Z-scan techniques. This allowed for different quantum yield state populations to be calculated such as ISC yields and lifetimes of the triplet/singlet excited states. When comparing PDs utilizing the heavy atom effect with sulfur and oxygen squaraine dye analogs, they found that the sulfur incorporated squaraine dyes provided the highest singlet oxygen production and the largest triplet quantum yields, approaching almost complete unity. This begged the question: why does this not translate into higher DNA photocleavage yields with Dye **1** at higher temperatures?

Peceli et al. also considered the instability of sulfur dyes in their paper which may explain the low photocleavage yields at room temperature shown with Dye **1** are likely attributable to short photobleaching times (i.e. short triplet state lifetimes caused by rapid photobleaching). Through the photobleaching vs. temperature absorption assay, it was determined that photobleaching times are remarkably augmented at lower temperatures likely due to decreased internal conversion pathway as exhibited by low-temperature fluorescence experiments in literature. Fluorescence has been shown to increase at lower temperatures which has been discussed as being analogous to increasing the density of the solution for fluorophores, resulting in limited rotational and vibrational deactivation pathways.³⁴ Ultimately, this could be viewed as akin to increased photocleavage yields at lower temperatures that are presented in this thesis. Therefore, increased photocleavage yields at low temperatures shows the potential of Dye **1** as an effective photosensitizing agent as long as the issues concerning photobleaching can be addressed through new, stable analogs.

The scavenger experiments reveal the involvement of relevant reactive oxygen species in the photocleavage mechanism of the DNA when near-infrared light is used to irradiate samples. This is necessary to show that oxygen still plays a contributing role even at lower temperatures and

within solid aqueous solutions. The observed decrease in photobleaching in conjunction with the potential involvement of sulfur radicals by the Dye **1** also indicate potential contributions to the photocleavage yields.

The binding mode studies (CD and photocleavage inhibition) indicate that more than one binding mode may be occurring for Dye **1**. To refine the specificity of binding interaction, an asymmetrical cyanine dye that incorporates sulfur is proposed and could be a possible path forward in improving photocleavage yields. By including a ring system that is prone to intercalation on one side of the cyanine dye, this could reduce any probable groove binding and aggregation phenomena. Moreover, this may result in higher anaerobic cleavage yields at higher temperatures by reducing oxygen interaction which is known to contribute to photobleaching.³⁴ Since it has been shown herein that sulfur radicals may be contributing to the photocleavage mechanism in the absence of oxygen, a precise intercalating mode could afford a photo-induced sulfur radical mechanism to dominate. This could have a potentially big impact given that many therapeutic agents in the treatment of cancer lack efficacy in oxygen-starved areas of tumors.

In summary, the reduced photobleaching observed at low temperatures combined with the unique nonradiative pathways exhibited by many sulfur-incorporated polymethines dyes may have resulted in increased photocleavage yields at low temperatures. At these temperatures, reduced photobleaching could also likely be accompanied by a decrease in vibronic relaxation, a known competitive pathway that depopulates the excited singlet and triplet states. These findings as well as increased photocleavage yields under hypoxic conditions represent a promising path forward in developing better dyes for applications in photodynamic therapy.

REFERENCES

1. Hamer, F. M., The cyanine dyes. *Quarterly Reviews, Chemical Society* **1950**, *4* (4), 327-355.
2. Fadda, A. A.; El-Mekawy, R. E., Some studies in cyanine dyes incorporating pyridine rings endowed with pharmaceutical potency. *Dyes and Pigments* **2015**, *118*, 45-52.
3. Shi, C.; Wu, J. B.; Pan, D., Review on near-infrared heptamethine cyanine dyes as theranostic agents for tumor imaging, targeting, and photodynamic therapy. *BIOMEDO* **2016**, *21* (5), 050901-050901.
4. Abrahamse, H.; Hamblin, M. R., New photosensitizers for photodynamic therapy. *The Biochemical journal* **2016**, *473* (4), 347-364.
5. Henary, M. M.; Mariusz, Stability and reactivity of polymethine dyes in solution. *Topics in Heterocyclic Chemistry* **2008**, *14*, 221-238.
6. Shindy, H. A., Fundamentals in the chemistry of cyanine dyes: A review. *Dyes and Pigments* **2017**, *145*, 505-513.
7. Yarmoluk, S. M.; Lukashov, S. S.; Losytsky, M. Y.; Akerman, B.; Korniyushyna, O. S., Interaction of cyanine dyes with nucleic acids. *Spectrochimica Acta Part A: Molecular and Biomolecular Spectroscopy* **2002**, *58* (14), 3223-3232.
8. Armitage, B. A., Cyanine Dye–DNA Interactions: Intercalation, groove binding, and aggregation. *DNA Binders and Related Subjects*, Waring, M. J.; Chaires, J. B., Eds. Springer Berlin Heidelberg: Berlin, Heidelberg, 2005; pp 55-76.
9. Karlsson, H. J.; Eriksson, M.; Perzon, E.; Åkerman, B.; Lincoln, P.; Westman, G., Groove-binding unsymmetrical cyanine dyes for staining of DNA: syntheses and characterization of the DNA-binding. *Nucleic Acids Research* **2003**, *31* (21), 6227-6234.
10. Narayanaswamy, N.; Das, S.; Samanta, P. K.; Banu, K.; Sharma, G. P.; Mondal, N.; Dhar, S. K.; Pati, S. K.; Govindaraju, T., Sequence-specific recognition of DNA minor groove by an NIR-fluorescence switch-on probe and its potential applications. *Nucleic Acids Research* **2015**, *43* (18), 8651-8663.
11. Jędrzejewska, B.; Bajorek, A.; Moraczewska, J., Interaction of carbocyanine dyes with DNA: Synthesis and spectroscopic studies. *Applied Spectroscopy* **2013**, *67* (6), 672-680.
12. Agostinis, P.; Berg, K.; Cengel, K. A.; Foster, T. H.; Girotti, A. W.; Gollnick, S. O.; Hahn, S. M.; Hamblin, M. R.; Juzeniene, A.; Kessel, D.; Korbelik, M.; Moan, J.; Mroz, P.; Nowis, D.; Piette, J.; Wilson, B. C.; Golab, J., Photodynamic therapy of cancer: an update. *CA: A Cancer Journal For Clinicians* **2011**, *61* (4), 250-281.
13. Tegos, G.; Dai, T.; Fuchs, B.; Coleman, J.; Prates, R.; Astrakas, C.; St Denis, T.; Ribeiro, M.; Mylonakis, E.; Hamblin, M., Concepts and principles of photodynamic therapy as an alternative antifungal discovery platform. *Frontiers in Microbiology* **2012**, *3*, 120.
14. Mehraban, N.; Freeman, S. H., Developments in PDT sensitizers for increased selectivity and singlet oxygen production. *Materials* **2015**, *8* (7).
15. Robertson, C. A.; Evans, D. H.; Abrahamse, H., Photodynamic therapy (PDT): A short review on cellular mechanisms and cancer research applications for PDT. *Journal of Photochemistry and Photobiology B: Biology* **2009**, *96* (1), 1-8.
16. Huang, Z., A review of progress in clinical photodynamic therapy. *Technology in Cancer Research & Treatment* **2005**, *4* (3), 283-293.
17. Yang, X.; Shi, C.; Tong, R.; Qian, W.; Zhau, H. E.; Wang, R.; Zhu, G.; Cheng, J.; Yang, V. W.; Cheng, T.; Henary, M.; Streckowski, L.; Chung, L. W. K., Near IR heptamethine cyanine dye-mediated cancer imaging. *Clinical Cancer Research* **2010**.

18. Peceli, D.; Hu, H.; Fishman, D. A.; Webster, S.; Przhonska, O. V.; Kurdyukov, V. V.; Slominsky, Y. L.; Tolmachev, A. I.; Kachkovski, A. D.; Gerasov, A. O.; Masunov, A. E.; Hagan, D. J.; Van Stryland, E. W., Enhanced intersystem crossing rate in polymethine-like molecules: Sulfur-containing squaraines versus oxygen-containing analogues. *The Journal of Physical Chemistry A* **2013**, *117* (11), 2333-2346.
19. Schore, N. E., Modern molecular photochemistry (Turro, Nicholas J.). *Journal of Chemical Education* **1981**, *58* (10), A312.
20. El-Sayed, M. A., Triplet state. Its radiative and nonradiative properties. *Accounts of Chemical Research* **1968**, *1* (1), 8-16.
21. Brown, J. M.; Wilson, W. R., Exploiting tumour hypoxia in cancer treatment. *Nature Reviews. Cancer* **2004**, *4* (6), 437-47.
22. Cui, J.; Mao, X.; Olman, V.; Hastings, P. J.; Xu, Y., Hypoxia and miscoupling between reduced energy efficiency and signaling to cell proliferation drive cancer to grow increasingly faster. *Journal of Molecular Cell Biology* **2012**, *4* (3), 174-176.
23. Lahiri, D.; Bhowmick, T.; Pathak, B.; Shameema, O.; Patra, A. K.; Ramakumar, S.; Chakravarty, A. R., Anaerobic photocleavage of DNA in red light by dicopper(II) complexes of 3,3'-dithiodipropionic acid. *Inorganic Chemistry* **2009**, *48* (1), 339-349.
24. Wauchope, O. R.; Shakya, S.; Sawwan, N.; Liebman, J. F.; Greer, A., Photocleavage of plasmid DNA by dibenzothiophene S-oxide under anaerobic conditions. *Journal of Sulfur Chemistry* **2007**, *28* (1), 11-16.
25. Lü, J. M.; Lin, P. H.; Yao, Q.; Chen, C., Chemical and molecular mechanisms of antioxidants: experimental approaches and model systems. *Journal of cellular and molecular medicine* **2010**, *14* (4), 840-860.
26. Ioele, M.; Steenken, S.; Baciocchi, E., Generation and reactivity of aromatic thioether radical cations in aqueous solution as studied by pulse radiolysis. *The Journal of Physical Chemistry A* **1997**, *101* (16), 2979-2987.
27. Fleming, S. A.; Jensen, A. W., Substituent effects on the photocleavage of benzyl– sulfur bonds. Observation of the “meta effect”. *The Journal of organic chemistry* **1996**, *61* (20), 7040-7044.
28. Becker, R. S.; Dolan, E.; Balke, D. E., Vibronic effects in photochemistry—competition between internal conversion and photochemistry. *The Journal of Chemical Physics* **1969**, *50* (1), 239-245.
29. Becker, R. S.; Favaro, G.; Romani, A.; Gentili, P. L.; Dias, F. M. B., Vibronic effects in pathways of photochemistry and vibrational relaxation. *Chemical Physics* **2005**, *316* (1–3), 108-116.
30. Meyer, B.; Phillips, L. F.; Smith, J. J., Temperature dependence of intersystem crossing: Lifetime and intensity of SO(2) phosphorescence in low-temperature Solids. *Proceedings of the National Academy of Sciences of the United States of America* **1968**, *61* (1), 7-11.
31. Song, L.; Fayer, M., Temperature dependent intersystem crossing and triplet-triplet absorption of rubrene in solid solution. *Journal of luminescence* **1991**, *50* (2), 75-81.
32. Leubner, I. H.; Hodgkins, J. E., Temperature dependence of the phosphorescence lifetime of benzene and n-alkylbenzenes between 4.2 and 100. deg. K. *The Journal of Physical Chemistry* **1969**, *73* (8), 2545-2550.
33. Kellogg, R. E.; Schwenker, R. P., “Temperature effect” on triplet state lifetimes in solid solutions. *The Journal of Chemical Physics* **1964**, *41* (9), 2860-2863.

34. Diaspro, A.; Chirico, G.; Usai, C.; Ramoino, P.; Dobrucki, J., Photobleaching. In *Handbook of biological confocal microscopy*, Springer: 2006; pp 690-702.
35. Zondervan, R.; Kulzer, F.; Kol'chenk, M. A.; Orrit, M., Photobleaching of rhodamine 6G in poly(vinyl alcohol) at the ensemble and single-molecule levels. *The Journal of Physical Chemistry A* **2004**, *108* (10), 1657-1665.
36. Andrews, D. L., *Photonics, Biomedical Photonics, Spectroscopy, and Microscopy*. John Wiley & Sons: 2015.
37. Firstov, S. V.; Alyshev, S. V.; Firstova, E. G.; Melkumov, M. A.; Khegay, A. M.; Khopin, V. F.; Guryanov, A. N.; Dianov, E. M., Dependence of the photobleaching on laser radiation wavelength in bismuth-doped germanosilicate fibers. *Journal of Luminescence* **2017**, *182*, 87-90.
38. Garbett, N. C.; Ragazzon, P. A.; Chaires, J. B., Circular dichroism to determine binding mode and affinity of ligand-DNA interactions. *Nat. Protocols* **2007**, *2* (12), 3166-3172.
39. Pascal, S.; Haefele, A.; Monnereau, C.; Charaf-Eddin, A.; Jacquemin, D.; Le Guennic, B.; Andraud, C.; Maury, O., Expanding the polymethine paradigm: Evidence for the contribution of a bis-dipolar electronic structure. *The Journal of Physical Chemistry A* **2014**, *118* (23), 4038-4047.
40. Singleton, D. L.; Paraskevopoulos, G.; Irwin, R. S., Rates and mechanism of the reactions of hydroxyl radicals with acetic, deuterated acetic, and propionic acids in the gas phase. *J. Am. Chem. Soc.* **1989**, *111* (14), 5248-5251.
41. Liu, J.; Li, J.; Dong, S., Interaction of brilliant cresyl blue and methylene green with DNA studied by spectrophotometric and voltammetric methods. *Electroanalysis* **1996**, *8* (8-9), 803-807.
42. Kellett, A.; O'Connor, M.; McCann, M.; McNamara, M.; Lynch, P.; Rosair, G.; McKee, V.; Creaven, B.; Walsh, M.; McClean, S.; Foltyn, A.; O'Shea, D.; Howe, O.; Devereux, M., Bis-phenanthroline copper(ii) phthalate complexes are potent in vitro antitumour agents with 'self-activating' metallo-nuclease and DNA binding properties. *Dalton Transactions* **2011**, *40* (5), 1024-1027.
43. Sundaravadivel, E.; Vedavalli, S.; Kandaswamy, M.; Varghese, B.; Madankumar, P., DNA/BSA binding, DNA cleavage and electrochemical properties of new multidentate copper(ii) complexes. *RSC Advances* **2014**, *4* (77), 40763-40775.

APPENDIX

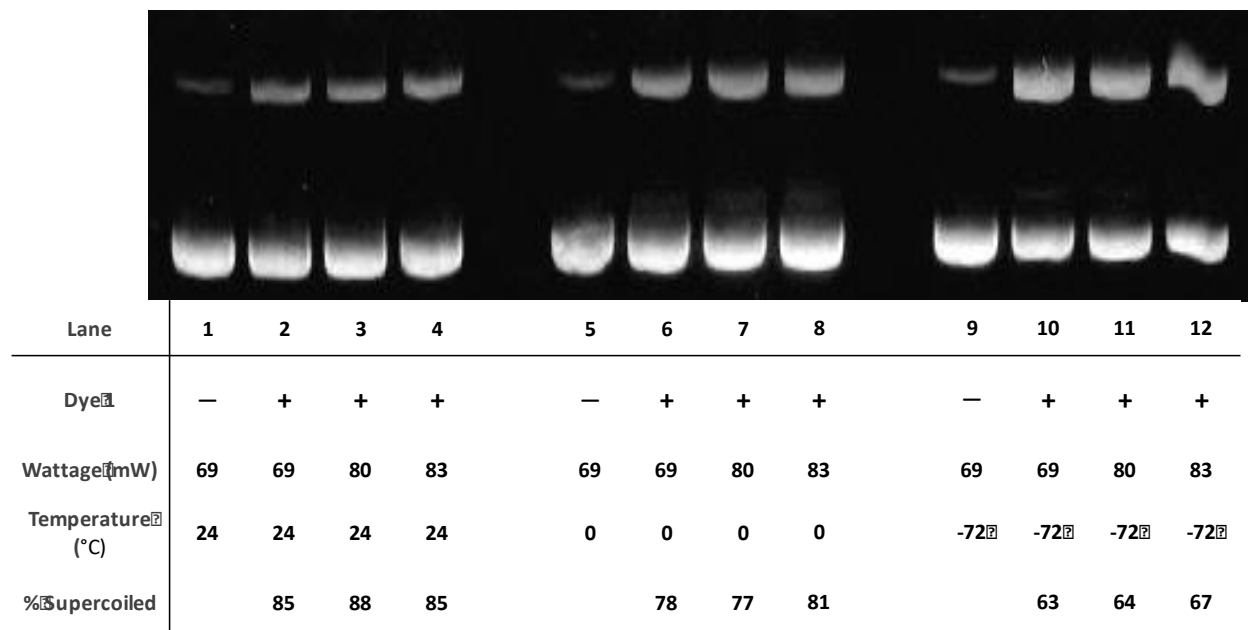


Figure 0.1: Trial #1 -- As the temperature conditions are decreased, an obvious increase in nicked and linear forms of plasmid DNA can be observed, indicating that either an indirect or direct correlation between temperature and photocleavage exists. Samples contained 38 μ M bp pUC 19, 10 mM phosphate buffer pH 7.0, and 50 μ M of Dye 1 or equal amounts of DMSO (Lanes 1, 5 and 9).

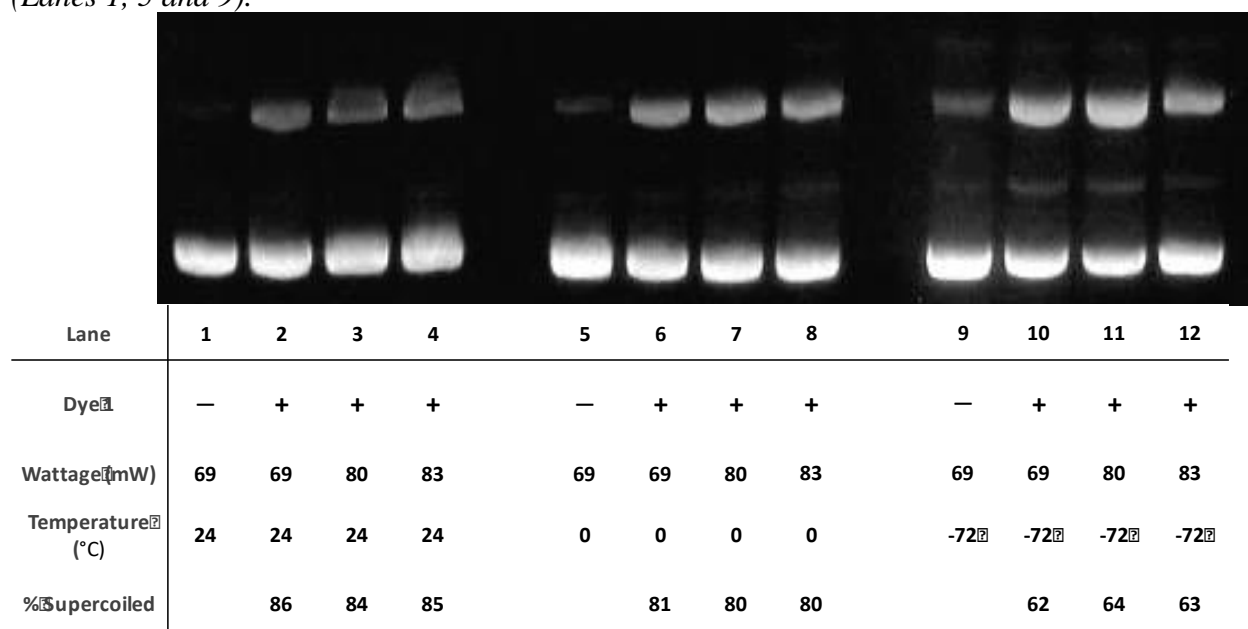


Figure 0.2: Trial #3 -- As the temperature conditions are decreased, an obvious increase in nicked and linear forms of plasmid DNA can be observed, indicating that either an indirect or direct correlation between temperature and photocleavage exists. Samples contained 38 μ M bp

pUC 19, 10 mM phosphate buffer pH 7.0, and 50 μ M of Dye 1 or equal amounts of DMSO (Lanes 1, 5 and 9).

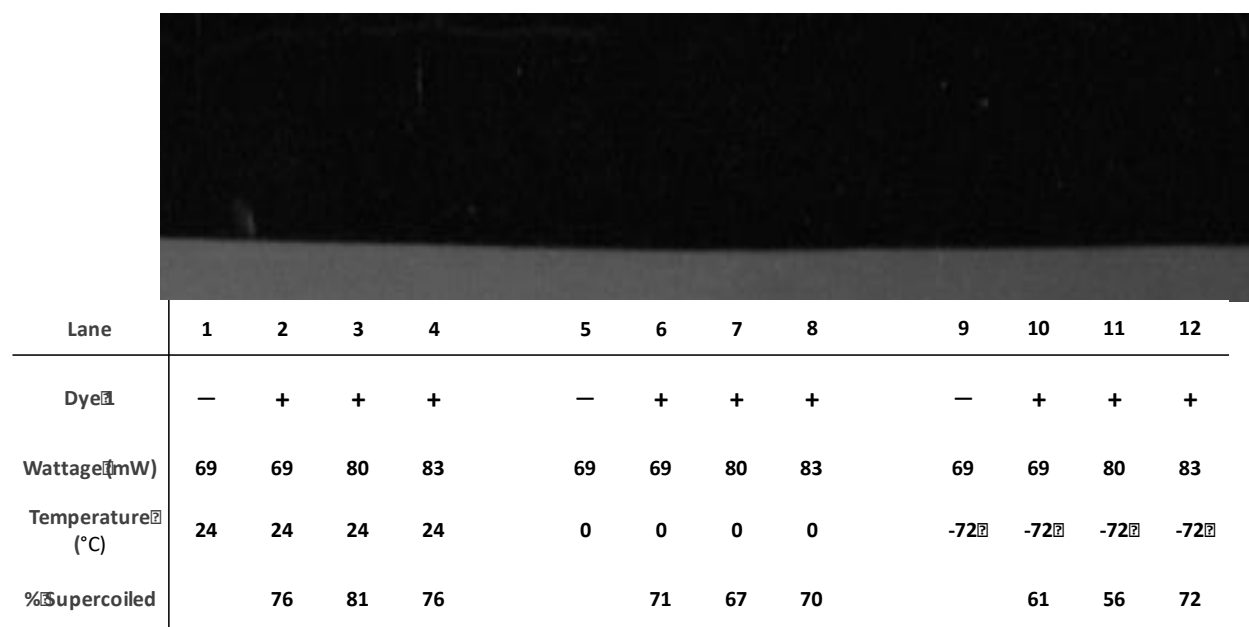


Figure 0.3: Trial #4 -- As the temperature conditions are decreased, an obvious increase in nicked and linear forms of plasmid DNA can be observed, indicating either an indirect or direct correlation between temperature and photocleavage exists. Samples contained 38 μ M bp *pUC19*, 10 mM phosphate buffer pH 7.0, and 50 μ M of Dye 1 or equal amounts of DMSO (Lanes 1, 5 and 9).

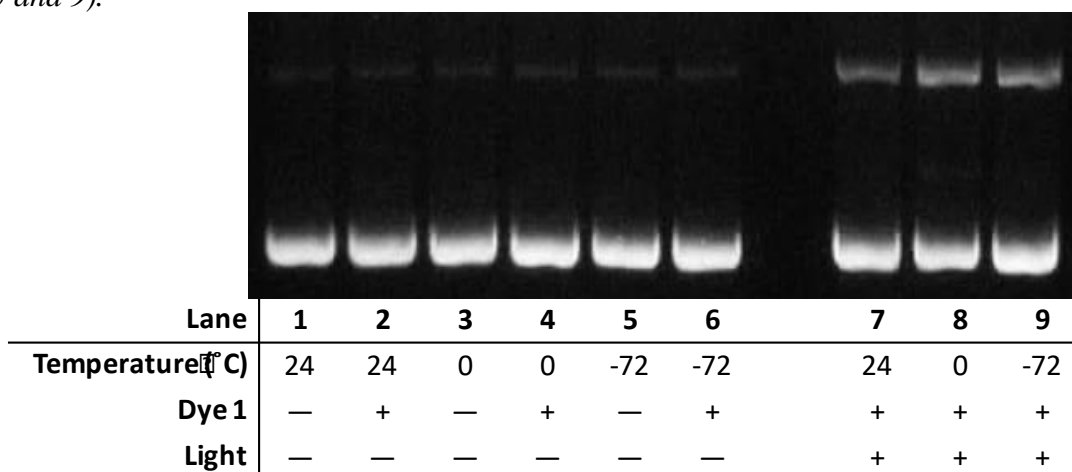


Figure 0.4: A dark control experiment over the three temperatures was done to show that only light within the Dye-DNA absorption spectrum contributed to the observed DNA cleavage. The samples consisted of 50 μ M Dye 1, 10 mM phosphate buffer pH 7.0, and 38 μ M bp *pUC19*. The references that did not contain Dye 1 had equal amounts of DMSO. Positive controls were incorporated as a reference.

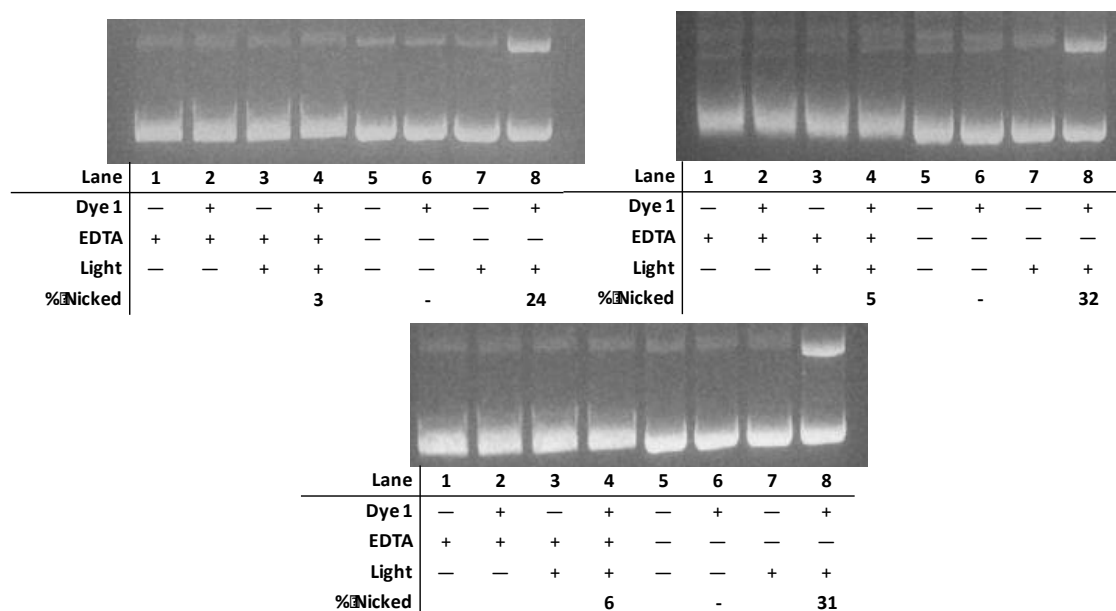


Figure 0.5: These three trials consisted Dye 1 (50 μ M) and/or EDTA (100 mM) in a 10 mM phosphate buffer pH 7.0 with 38 μ M bp pUC19. Two samples containing the inhibitor and two samples containing Dye 1 were irradiated using an 83 mW 780 nm laser for 30 min at -72 $^{\circ}$ C. Dark controls were also kept at -72 $^{\circ}$ C for 30 min.

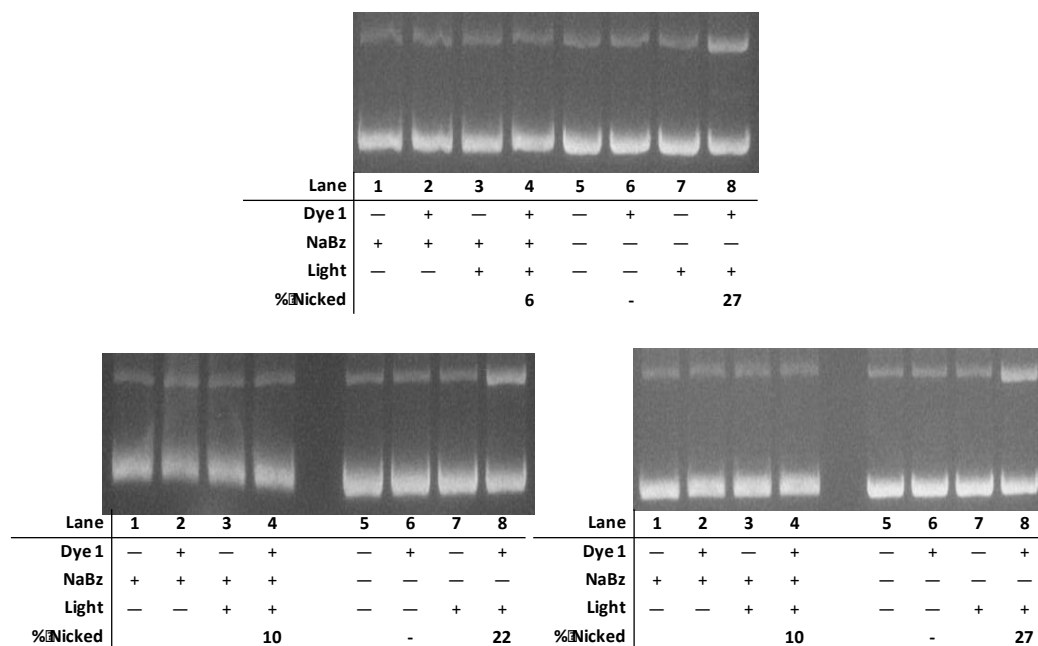


Figure 0.6: These three trials consisted of Dye 1 (50 μ M) and/or sodium benzoate (100 mM) in a 10 mM phosphate buffer pH 7.0 with 38 μ M bp pUC19. Two samples containing the inhibitor and two samples containing Dye 1 were irradiated using an 83 mW 780 nm laser for 30 min at -72 $^{\circ}$ C. Dark controls were also kept at -72 $^{\circ}$ C for 30 min.

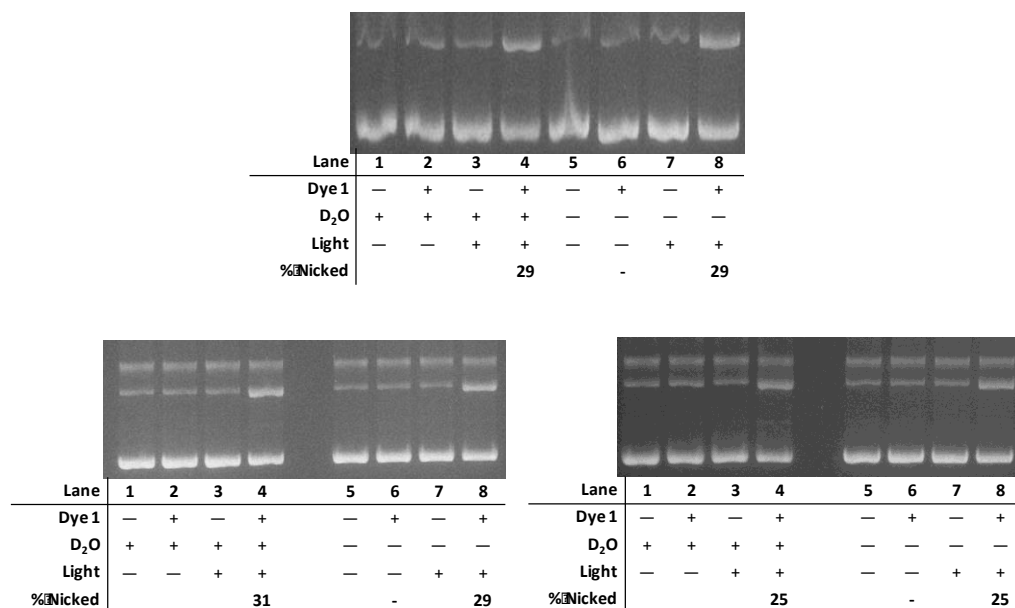


Figure 0.7: These three trials consisted of either 76% D₂O or dH₂O in a 10 mM phosphate buffer pH 7.0 with 38 μ M bp pUC19 and 50 μ M of Dye 1. Two samples containing D₂O with Dye 1 and two samples containing dH₂O with Dye 1 were irradiated using an 83 mW 780 nm laser for 30 min at -72 $^{\circ}$ C. Dark controls were also kept at -72 $^{\circ}$ C for 30 min.

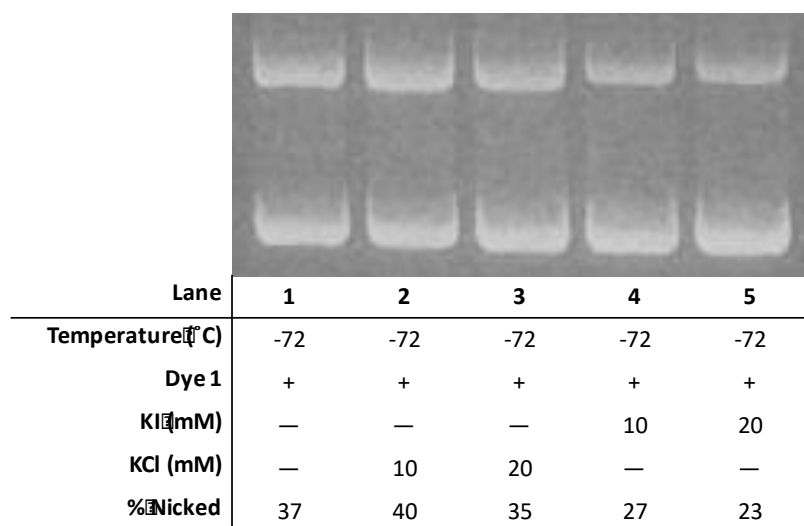


Figure 0.8: This single trial consisted of Dye 1 (70 μ M) and/or potassium iodide or potassium chloride (10 mM and 20 mM) in a 10 mM phosphate buffer pH 7.0 with 38 μ M bp pUC19. All samples were irradiated using an 83 mW 780 nm laser for 30 min at -72 $^{\circ}$ C.

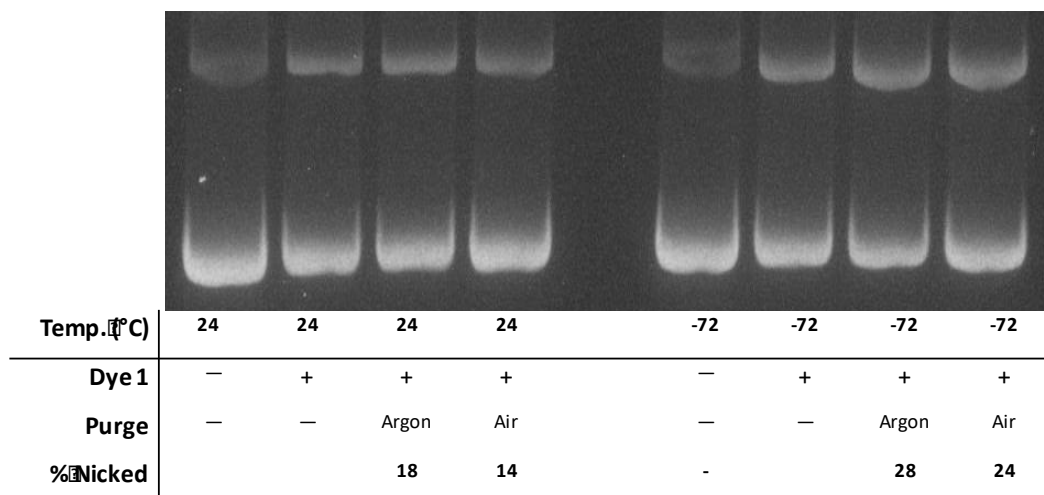


Figure 0.9: Trial #2 -- The photocleavage experiment using air and argon purging to purged with argon or air for 1 min. Samples containing 70 μM Dye 1 or equal amounts of DMSO (Lanes 1 and 5), 10 mM phosphate buffer pH 7.0, and 38 μM bp pUC19 were irradiated using 780 nm 83 mW lasers for 30 min after adjusting to the appropriate temperature.

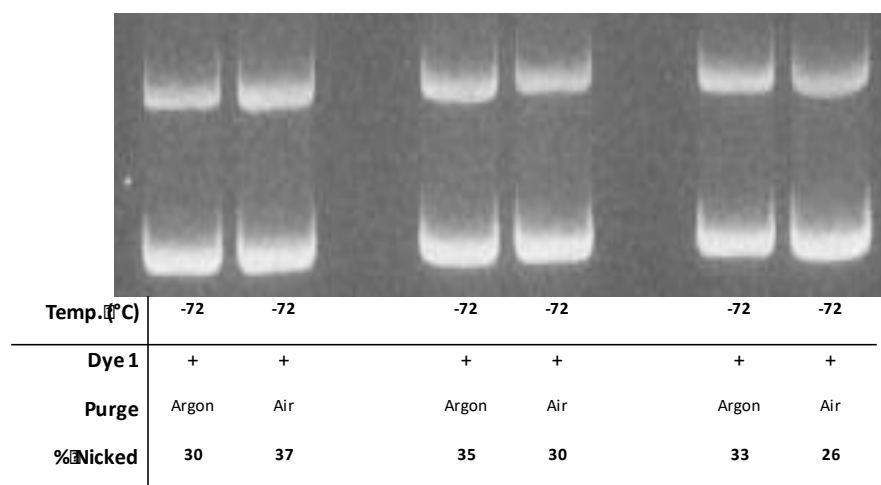


Figure 0.10: Trials 3,4, and 5 -- The photocleavage experiment using air and argon purging to determine the role molecular oxygen plays in the photocleavage mechanism. Samples were gently purged with argon or air for 1 min. Samples containing 70 μM Dye 1, 10 mM phosphate buffer pH 7.0, and 38 μM bp pUC19 were irradiated using 780 nm 83 mW lasers for 30 min after adjusting to the appropriate temperature. These three trials were only done at -72 °C.

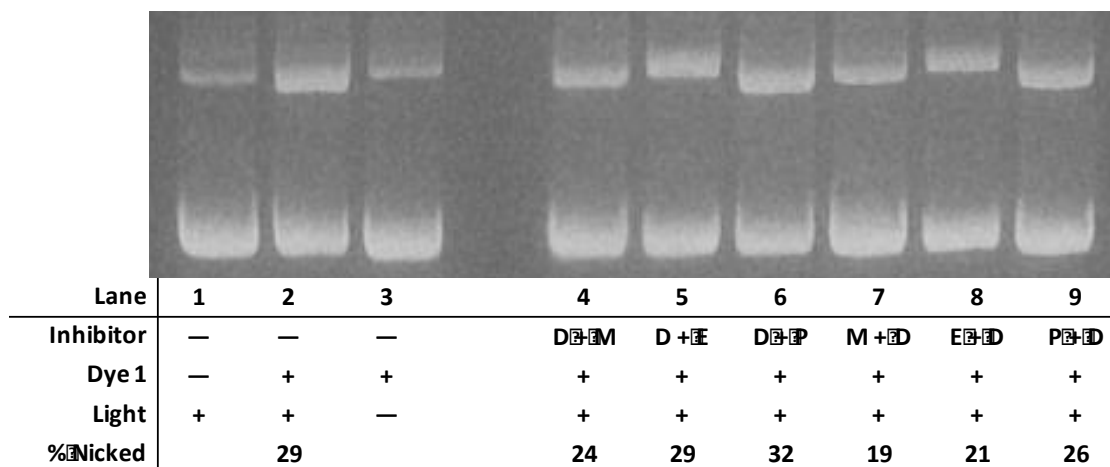


Figure 0.11: Trial 2 -- The photocleavage experiment using air and argon purging to determine the role molecular oxygen plays in the photocleavage mechanism. Samples were gently purged with argon or air for 1 min. Samples containing 70 μ M Dye 1 or equal amounts of DMSO (Lanes 1 and 4), 10 mM phosphate buffer pH 7.0, and 38 μ M bp pUC19 were irradiated using 780 nm 83 mW lasers for 30 min after adjusting to the appropriate temperature.

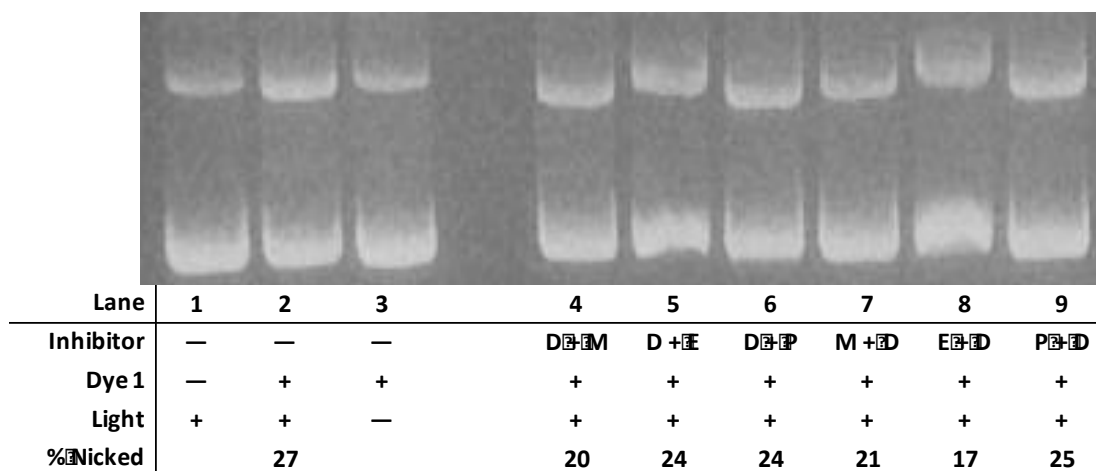


Figure 0.12: Trial 3 -- The photocleavage experiment using air and argon purging to determine the role molecular oxygen plays in the photocleavage mechanism. Samples were gently purged with argon or air for 1 min. Samples containing 70 μ M Dye 1 or equal amounts of DMSO (Lanes 1 and 4), 10 mM phosphate buffer pH 7.0, and 38 μ M bp pUC19 were irradiated using 780 nm 83 mW lasers for 30 min after adjusting to the appropriate temperature.

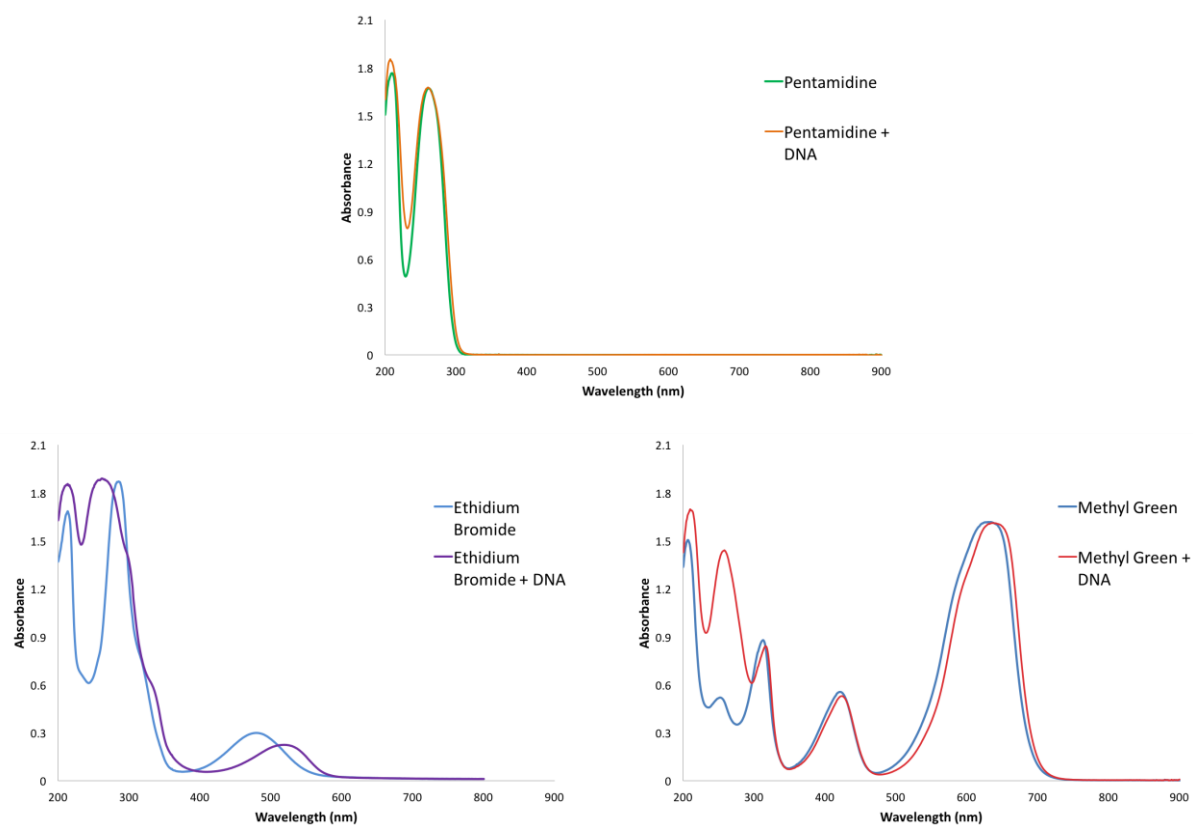


Figure 0.13: Absorption spectra of the inhibitor reagents used in the photocleavage binding assay in the presence and absence of 100 μM bp CT-DNA in 10 mM phosphate buffer pH 7.0. The concentration of each inhibitor is 50 μM (All spectra recorded by Kanchan Basnet.)